Interaction of an α-synuclein epitope with HLA-DRB1*15:01 triggers enteric features in mice reminiscent of prodromal Parkinson's disease

Francesca Garretti[1, 2, 10, 11†], Connor Monahan[2, 10†], Nicholas Sloan[3], Jamie Bergen[3, 4], Sanjid Shahriar[1], Seon Woo Kim[5], Alessandro Sette[6, 7, 10], Tyler Cutforth[8, 10], Ellen Kanter[2, 9], Dritan Agalliu[1, 8, 10, *] and David Sulzer[2, 8, 9, 10, *]

1. Department of Pathology and Cell Biology, Columbia University Irving Medical Center, New York, NY, USA.

2. Departments of Psychiatry and Pharmacology, Columbia University Irving Medical Center, New York, NY, USA.

3. Department of Neuroscience, Columbia University, New York, NY, USA.

4. Department of Computer Science, Columbia University, New York, NY, USA.

5. Weill Cornell Medicine - Qatar, Education City, Doha, Qatar.

6. Division of Vaccine Discovery, La Jolla Institute for Immunology, La Jolla, CA, USA.

7. Department of Medicine, University of California in San Diego, San Diego, CA, USA.

8. Department of Neurology, Columbia University Irving Medical Center, New York, NY, USA.

9. Division of Molecular Therapeutics, New York State Psychiatric Institute, New York, NY, USA.

10. Aligning Science Across Parkinson's (ASAP) Collaborative Research Network, Chevy Chase, MD, USA.

11. Present address: Department of Genetics and Genomics, Icahn School of Medicine at Mount Sinai, New York, NY, USA.

[†] Equal contribution authorship

* Correspondence: David Sulzer: ds43@cumc.columbia.edu

Dritan Agalliu: da191@cumc.columbia.edu

SUMMARY

Enteric symptoms, including constipation, are hallmarks of prodromal Parkinson's disease (PD) that can appear decades before the onset of motor symptoms and diagnosis. PD patients possess circulating T cells that recognize specific α-synuclein-(α-syn)-derived epitopes. One epitope, α-syn$_{32-46}$, binds with strong affinity to the HLA-DRB1*15:01 allele implicated in autoimmune diseases. We report that α-syn$_{32-46}$ immunization in a mouse expressing HLA-DRB1*15:01 triggers intestinal inflammation leading to loss of enteric neurons, damage of enteric dopaminergic neurons, constipation and weight loss. α-Syn$_{32-46}$ immunization activates innate and adaptive immune gene signatures in the gut and induces changes in CD4$^+$ T$_H$1/ T$_H$17 transcriptome that resemble tissue resident memory cells found in mucosal barriers during inflammation. Depletion of CD4$^+$, but not CD8$^+$, T cells partially rescues enteric neurodegeneration. Therefore, interaction of α-syn$_{32-46}$ and HLA-DRB1*15:0 is critical for gut inflammation and CD4$^+$ T cell-mediated loss of enteric neurons in humanized mice, suggesting potential mechanisms of prodromal enteric PD.

KEYWORDS

Parkinson's disease; α-synuclein; neo-antigen; HLA-DRB1*15:01; prodromal disease; enteric dopaminergic neurons; constipation; CD4$^+$ T cells; antigen-experienced T$_{RM}$; mucosal barriers.

HIGHLIGHTS AND eTOC Blurb

1. α-syn$_{32-46}$ immunization of an HLA-DRB1*15:01 mouse triggers weight loss and constipation.
2. α-syn$_{32-46}$ immunizations induce gut inflammation, loss of enteric neurons and damage to dopaminergic neurons.
3. α-syn$_{32-46}$ immunization induces innate and adaptive immune responses in the gut.

4. Depletion of $CD4^+$, but not $CD8^+$, T cells partially rescues enteric neural loss.
5. An interaction between α-syn_{32-46} and HLA-DRB1*15:01 is critical for this model of prodromal PD.

Parkinson's disease (PD) patients exhibit elevated number of circulating T cells that recognize α-synuclein-(α-syn)- epitopes, particularly during early disease stages. One epitope, α-syn_{32-46}, interacts with the HLA-DRB1*15:01; however, its role in PD pathogenesis remains unknown. Garretti *et al*. show that α-syn_{32-46} immunization of a mouse expressing HLA-DRB1*15:01 triggers intestinal inflammation, a loss of enteric neurons, constipation and weight loss, suggesting a critical role for α-syn autoimmunity in HLA-DRB1*15:01 carriers in prodromal PD.

INTRODUCTION

Parkinson's disease (PD) is a neurodegenerative disorder characterized by prominent motor symptoms resulting from the loss of central nervous system (CNS) dopaminergic neurons located in the substantia nigra (SN) (Fahn and Sulzer, 2004). However, pathogenic steps in PD begin long before diagnosis, and the death of these neurons is suspected to occur at relatively late stages of disease pathogenesis. In contrast, enteric nervous system (ENS) symptoms are common during an earlier prodromal stage of the disease (Heinzel et al., 2019). Constipation presents in approximately 70% of PD patients (Fasano et al., 2015), is three-fold more prevalent in PD patients than healthy controls (Drossman, 2006), and may occur as early as twenty years prior to the onset of motor symptoms (Khoo et al., 2013). Although epidemiological studies have demonstrated a high prevalence of constipation in PD patients [reviewed in (Fasano et al., 2015)], and postmortem studies indicate that gut pathology is present before the onset of motor symptoms (Braak et al., 2003; Stokholm et al., 2016), the mechanisms underlying the enteric pathophysiology remain unclear.

Braak and colleagues have hypothesized that α-synuclein (α-syn) -mediated pathology begins in the ENS and subsequently ascends rostrally into the brain via the vagus nerve (Braak et al., 2003). This conjecture is consistent with reports that truncal vagotomies decrease the risk for PD (Liu et al., 2017; Svensson et al., 2015; Tysnes et al., 2015). Epidemiological studies support a role for gut inflammation in early stages of PD. The incidence of PD among patients with inflammatory bowel disease (IBD) is 28% higher than controls. Furthermore, IBD patients who receive anti-TNFα therapy exhibit a 78-100% reduction in PD incidence compared to those who do not receive such therapy (Park et al.; Peter et al., 2018). Multiple observations in animal models are also consistent with the hypothesis that gut inflammation may be involved in the early stages of PD-like pathogenesis [reviewed in (Metzger and Emborg, 2019)].

A possible role for peripheral inflammation in PD pathogenesis is suggested by findings that increased levels of pro-inflammatory cytokines (e.g., TNFα, IL-1β, IL-6 and IFNγ) are found in PD patients and correlate negatively with disease duration (Cossais et al., 2021; Devos et al., 2013; Pochard et al., 2018; Qin et al., 2016). PD patients also possess circulating T cells, mostly $CD4^+$ subtypes, that recognize specific α-syn-derived neo-epitopes (Sulzer et al., 2017). These cells are present at particularly high levels during the first decade following diagnosis and likely during the prodromal phase prior to the onset of motor symptoms and clinical diagnosis (Lindestam Arlehamn et al., 2020). Thus, α-syn neo-antigen reactivity may be relevant to the prodromal and early stages of PD [reviewed in (Garretti et al., 2019)]. However, the role of α-syn neo-antigen reactivity in disease etiology remains unknown.

Previously, we reported that most α-syn-responsive $CD4^+$ T cells isolated from PD patients respond to epitopes derived from two regions of the protein (Sulzer et al., 2017). One region requires the presence of phosphorylated amino acid serine 129 (Sulzer et al., 2017), a post-translational modification present at high levels in Lewy bodies (Fujiwara et al., 2002). However, these C-terminal epitopes bind weakly to several human leukocyte antigen (HLA) alleles, indicating that they are "unrestricted". The other major α-syn epitope identified in PD patients is the peptide α-syn_{32-46}, which lies in proximity to several rare α-syn mutations that cause familial PD (Appel-Cresswell et al., 2013; Ki et al., 2007; Kruger et al.; Lesage et al., 2013; Liu et al., 2021; Pasanen et al., 2014; Polymeropoulos et al., 1997; Yoshino et al., 2017; Zarranz et al., 2004). In contrast to the C-terminal epitopes, the α-syn_{32-46} epitope is highly restricted to a specific HLA haplotype [B*07:02, C*07:02, DRB5*01, DRB1*15:01, DQA1*01:02, DQB1*06:02], expressed by approximately one third of the population (Sulzer et al., 2017). Importantly, there is a very strong binding affinity (K_D=2.8 nM) of the peptide to HLA-DRB1*15:01 *in vitro* (Sulzer et al., 2017). Independent genome-wide association studies (GWAS) have also confirmed that this haplotype is associated with PD (Hamza et al., 2010; Hill-Burns et al., 2011; Kannarkat et al., 2015).

It is unknown how the interaction between this α-syn epitope (α-syn$_{32-46}$) and HLA allele (DRB1*15:01) may trigger early features of PD. Here, we report that α-syn$_{32-46}$ peptide immunizations of a mouse strain lacking the mouse MHC-II alleles and expressing the human HLA-DRB1*15:01 allele trigger intestinal inflammation and loss of enteric neurons in the submucosal plexus of the small intestine leading to constipation and weight loss; however, there were no detectable effects in the CNS. Bulk RNA sequencing revealed that α-syn$_{32-46}$ immunizations induced transcriptome changes in the gut related to innate and adaptive immune responses and interferon signaling. Single cell RNA sequencing (scRNAseq) of immune cells showed altered gene signatures in CD4$^+$ T$_H$1 and T$_H$17 lamina propria lymphocytes of CFA/α-syn$_{32-46}$ -immunized mice. These cells adopted a transcriptome signature characteristic of antigen-experienced tissue resident memory cells found in mucosal barriers during infection and chronic inflammation. These enteric pathologies and symptoms were not observed in wild-type mice immunized with the same peptide, indicating a specificity of the immune response to a specific MHC-II genotype. Depletion of CD4$^+$, but not CD8$^+$, T cells partially rescued enteric neurodegeneration. Thus, interactions of α-syn$_{32-46}$ peptide with the HLA-DRB1*15:01 allele are critical for the induction of enteric features resembling those found in prodromal PD, and suggest that additional hits (e.g., blockade of intracellular protein turnover and/or α-syn aggregation) may be required for development of CNS symptoms.

RESULTS

α-Syn$_{32-46}$ immunizations cause illness marked by severe weight loss and constipation in HLA-DRB1*15:01, but not wild-type, mice.

Previously, we have shown that CD4$^+$ T cells isolated from PD patients carrying the HLA-DRB1*15:01 allele confer a strong immune response to the α-syn$_{32-46}$ region of the protein (Sulzer et al., 2017). To test if anti-α-syn$_{32-46}$ immune responses identified in PD patients can produce features of PD pathology in mice, we performed active immunizations by adapting a protocol similar to the myelin oligodendrocyte

glycoprotein (MOG_{35-55}) experimental autoimmune encephalomyelitis (EAE) mouse model for human multiple sclerosis (Lengfeld et al., 2017; Lutz et al., 2017). Mice were immunized with either PBS with CFA (complete Freund's adjuvant), or α-syn_{32-46} with CFA (referred to as CFA and CFA/α-syn_{32-46} immunization, respectively). As in EAE, *Bordetella pertussis* (*B. pertussis*) toxin was administered intravenously at 14 and 16 days post-initial immunization (DPI) with the boost to transiently open the blood-brain barrier in order to permit immune cell infiltration into the CNS (**Figure 1A**). In addition, mice were injected with PBS alone to control for the effects of CFA administration (referred to herein as PBS). These immunizations were performed either in C57BL/6J [referred to as wild-type (WT)] mice, or a humanized mouse strain lacking the mouse MHC-II alleles and expressing the human HLA-DRB1*15:01 allele [referred to as the HLA mice (Finn et al., 2004; Khare et al., 2005)] (**Figure 1A**). We confirmed that splenocytes from HLA-DRB1*15:01 mice expressed HLA-DR protein, and that its expression was increased when these cells were exposed to lipopolysaccharide (LPS) (**Figure S1A-G**). HLA-DR protein was not detected in WT splenocytes, as expected (**Figure S1H, I**). In addition, we confirmed that HLA mice expressed similar proportions of $CD4^+$ and $CD8^+$ T cells to WT mice (**Figure S1J-L**).

Mice were monitored daily for overt signs of malaise or weight changes (**Figure 1B-E**). Mice were categorized as "sick" if they lost more than 12% of the initial body weight and exhibited hunched posture with ungroomed and "ruffled" fur (**Figure 1B**). Following immunizations, very few WT mice became sick regardless of the antigen used for immunization (0% of CFA; 4% CFA/α-syn_{32-46}; **Figure 1B, C**). In contrast, while CFA alone produced no illness in HLA mice, 25% of HLA mice immunized with CFA/α-syn_{32-46} became ill or died (**Figure 1B, D**). The "sick" CFA/α-syn_{32-46}-immunized HLA mice exhibited severe weight loss starting at 16 DPI that peaked at 22- 24 DPI, with a mean weight change of -15.68 % at 22 DPI ($p= 0.0272$; **Figure 1E**). The weight effects seen with CFA/α-syn_{32-46} immunization were specific to HLA mice and were absent in WT mice (**Figure 1C**). This phenotype was transient: sick

HLA-immunized mice restored their initial weight between 24 - 29 DPI, with no further weight gain (**Figure 1E**).

As constipation is often an early symptom associated with PD that occurs as early as 20 years prior to the onset of motor symptoms (Khoo et al., 2013), we assessed total gastrointestinal transit time in either PBS, CFA, or CFA/α-syn$_{32-46}$-immunized mice by measuring the time required for a non-absorbable red dye to be excreted with feces after oral administration (**Figure 2A, B**). We selected three times points after immunization (21, 25 and 35 DPI) to correlate this phenotype with the weight loss (**Figure 1E)**. Immunizations with CFA had a significant effect on total GI transit time (PBS vs CFA, $p= 0.0029$; PBS vs CFA/α-syn$_{32-46}$ $p<0.0001$; **Figure 2C, D**). While the GI transit time between all CFA/α-syn$_{32-46}$- and CFA-immunized HLA mice at 21 DPI was not significantly different ($p= 0.1473$; **Figure 2C**), the sick CFA/α-syn$_{32-46}$ HLA mice displayed significantly longer GI transit time compared to both PBS and CFA mice ($p< 0.0001$; **Figure 2D**). The increase in GI transit time, however, recovered by 25 and 35 DPI (**Figure 2E, F**), mirroring the recovery from weight loss (**Figure 1E**). Interestingly, all CFA/α-syn$_{32-46}$ HLA mice showed a significant negative correlation between the peak weight loss and GI transit time ($r= -0.5643$, $p= 0.0077$; **Figure 2H**), whereas this was not seen with CFA-immunized HLA mice (peak weight loss and GI transit time; $r= 0.3188$, $p= 0.1707$; **Figure 2G**). In contrast, all immunized WT mice exhibited unaltered total GI transit times, regardless of the immunization antigen, indicating a specificity of the immune response (**Figure 2I**). Thus, the combination of α-syn$_{32-46}$ peptide and HLA-DRB1*15:01 allele expression induces acute gastrointestinal illness (weight loss and constipation) between 22-24 DPI.

α-Syn$_{32-46}$-immunized HLA mice exhibit loss of the enteric, but not central nervous system, neurons.

The weight loss associated with constipation observed in CFA/α-syn$_{32-46}$-immunized HLA mice suggests a pathological response targeting the gut. To examine the gut histopathology underlying these

phenotypes, we prepared flat mounts of both the submucosal and myenteric plexuses of the ileum (small intestine) from immunized HLA mice at 28 DPI (**Figure 3A, B**), since this preparation provides an in-depth analysis of the ENS. We focused in particular on the submucosal plexus since it is directly exposed to circulating immune cells and has the highest concentration of dopaminergic neurons (Li et al., 2004). To investigate whether the increase in total GI transit time was associated with neuronal loss, we analyzed expression of ANNA1 as a marker for enteric neuronal nuclei, and tyrosine hydroxylase (TH) as a marker for catecholaminergic neurons, which in the ileum are mostly dopaminergic (Li et al., 2004).

In the myenteric plexus, there was a similar density of ANNA1$^+$ neurons among PBS, CFA, and CFA/α-syn$_{32-46}$ - immunized HLA mice (**Figure 3C-E, I**). The CFA immunization reduced the overall TH$^+$ neuron density in the myenteric plexus (PBS vs CFA, p= 0.005; PBS vs CFA/α-syn$_{32-46,}$ p=0.006; **Figure 3J**), consistent with adjuvant effects on total GI transit time (**Figure 2C, D**). In contrast, CFA/α-syn$_{32-46}$-immunized HLA mice exhibited a significantly reduced ANNA-1$^+$ neuronal density in the submucosal plexus compared to CFA-immunized HLA mice (p= 0.04, **Figure 3F-H, K**)**;** however, there was no significant difference in ANNA-1$^+$ neurons between PBS and CFA-immunized mice (**Figure 3K).** There was no significant difference in the number of TH$^+$ neurons within the submucosal plexus in any group (**Figure 3L,** p= 0.260), which may be due to the variable density of TH$^+$ neurons, despite the large areas of the ENS encompassed by the flat mount analysis. Importantly, the area of TH$^+$ processes was significantly lower in CFA/α-syn$_{32-46}$-immunized compared to PBS-injected HLA mice (**Figure 3M**, p=0.008), although there was no significant difference between CFA and CFA/α-syn$_{32-46}$-immunized HLA mice (**Figure 3M**; p= 0.181). Similarly, the mean fluorescent intensity (MFI) of TH label within neuronal cell bodies and processes at 28 DPI was significantly lower in CFA/α-syn$_{32-46}$ immunized than PBS HLA mice (**Figure 3N,** p= 0.017), although there was no significant difference between CFA and CFA/α-syn$_{32-46}$-immunized HLA mice (**Figure 3N**; p= 0.171). The effects of CFA/α-syn$_{32-46}$-immunizations on enteric neuronal loss were specific to HLA mice, and not seen in WT mice (**Figure**

S2). Thus, α-syn$_{32-46}$ immunizations induced loss of enteric neurons in the ileum only in the HLA-DRB1*15:01 strain.

The submucosal plexus is exposed to circulating immune cells including T lymphocytes (**Figure 3B**) (Yoo and Mazmanian, 2017). To determine if the enteric neuron loss observed in CFA/α-syn$_{32-46}$ immunized HLA mice correlates with immune cell infiltration, we immunolabeled and quantified Iba1^{+}/CD68^{+} macrophages in these layers (**Figure S3**). We found no significant difference in CD68^{+} macrophage density in either the myenteric (**Figure S3 A-C, G**), or the submucosal (**Figure S3 D-F, H**) plexuses of the HLA mice regardless of the immunizing condition. Thus, the loss of enteric neurons does not correlate with the macrophage number in CFA/α-syn$_{32-46}$ -immunized HLA mice.

Next, we examined whether CFA/α-syn$_{32-46}$-immunized HLA mice exhibiting weight loss and constipation had CNS pathology. α-Syn$_{32-46}$ immunizations did not induce CD3^{+} T cell infiltration, microglia activation, macrophage infiltration, or loss of SN dopaminergic neurons in the brains of either WT or HLA mice, up to two months after immunization (70 DPI; **Figure S4A-O**). Consistently, neither WT nor HLA mice displayed motor behavior or learning deficits after α-syn$_{32-46}$ immunizations (**Figure S4P-Y**). The lack of CNS lymphocyte infiltration, neuroinflammation and neurodegeneration coupled with no changes in either motor skills or learning behaviors indicate that the severe weight loss and constipation in α-syn$_{32-46}$-immunized HLA mice are likely not related to changes in basal ganglia circuits. Therefore, the responses to α-syn$_{32-46}$ immunizations were restricted to the ENS in HLA mice.

Dopaminergic neuron damage in the gut corresponds to and persists after the weight loss in α-syn$_{32-46}$ - immunized HLA mice

To uncover the chronology between weight loss, gut inflammation and ENS neuronal death in CFA/α-syn$_{32-46}$-immunized HLA mice, we analyzed the number of ANNA1$^+$ and TH$^+$ neurons in the myenteric and submucosal plexuses at 18 and 42 DPI (**Figure 4A and B**), prior to and after the weight loss (**Figure 1E**). At 18 DPI, there was no difference in the number of ANNA1$^+$ neurons, dopaminergic neurons or TH$^+$ fluorescence signal in the submucosal plexus between CFA and CFA/α-syn$_{32-46}$-immunized HLA mice (**Figure 4E, F, J-L**). At 42 DPI, the area and MFI of the TH$^+$ signal were both significantly decreased in the submucosal plexus of CFA/α-syn$_{32-46}$ compared to CFA-immunized HLA mice ($p= 0.0135$ and $p= 0.0066$, respectively; **Figure 4O, P, U, V**), with no significant difference in the number of either ANNA1$^+$ or dopaminergic TH$^+$ neuronal bodies ($p= 0.226$; **Figure 4O, P, T**). There were no changes in any of these parameters in the myenteric plexus at 18 or 42 DPI (**Figure 4C, D, G, H, M, N, Q, R**). There was also no significant difference in the number of macrophages in the myenteric and submucosal plexuses at 18 and 42 DPI between CFA and CFA/α-syn$_{32-46}$-immunized HLA mice (**Figure S3I-T**), suggesting no relationship between macrophage number and ENS neuron loss. Overall, the time course analysis indicates that damage of TH$^+$ dopamine neurons in the submucosal plexus of CFA/α-syn$_{32-46}$- immunized HLA mice began prior to 28 DPI, and persisted by day 42 DPI, after the mice have recovered from the weight loss, independent of macrophage infiltration in the gut.

α-Syn$_{32-46}$ immunization activates innate and adaptive immune gene signatures in the gut

To investigate the mechanisms underlying the gut inflammation in CFA/α-syn$_{32-46}$ -immunized HLA mice, we performed bulk RNA sequencing and differential gene expression analysis of the ileum between CFA/α-syn$_{32-46}$ and CFA-immunized HLA mice at 21 DPI, when mice showed the largest weight loss (**Figure 5A; Table S1**). Differential gene expression analysis identified 143 upregulated, and 54 downregulated genes in CFA/α-syn$_{32-46}$ - immunized HLA mice (**Figure 5B**; $p_{adj} < 0.05$ and $|\log_2 fc| > 0.5$; **Table S1B- D**). Gene ontology (GO) enrichment analysis using the Database for Annotation,

Visualization and Integrated Discovery (DAVID) revealed significant GO terms for genes with similar functional characteristics upregulated in CFA/α-syn$_{32-46}$ immunized HLA mice such as: a) the innate immune response (*e.g.*, GO: 0045087, FDR = 2.34 x 10^{-25}); b) the response to interferon-β (GO: 0035456, FDR = 3.64 x 10^{-15}) including interferon-stimulated genes (*Stat1/2*, *Oas2*, *Irf7*, and *Isg15*) that play multiple roles in defense against pathogens; and c) the response to cytokines (GO: 0034097, FDR = 3.54 x 10^{-16}) including several chemokines (e.g., *Cxcl10* and *Cxcl13*) and *Vcam1*, a cell adhesion molecule involved in immune cell adhesion to blood vessels (**Figure 5C; Table S1E**). Additionally, genes involved in lymphocyte-mediated immunity (GO: 0002449, FDR = 0.00593) were also significantly enriched including antigen processing and presentation via MHC class I (*Tap1*, *H2.T24*, *H2.Q6*, *H2.T22*, *H2.T23*) (**Figure 5C; Table S1E**). Finally, humoral immune response was a significant GO term (GO: 0002455, FDR = 0.0495) with upregulation of genes encoding for the immunoglobulin heavy chain and complement cascade (**Figure 5C; Table S1E**). Thus CFA/α-syn$_{32-46}$ immunizations upregulated innate and adaptive immune gene signatures in the ileum of HLA mice at peak weight loss and constipation.

α-Syn$_{32-46}$-specific T cells are present in the lymphatic organs of WT, but not HLA-DRB1*15:01 mice, after immunization

Since CFA/α-syn$_{32-46}$ immunizations upregulate innate and adaptive immune gene signatures in the ileum of HLA mice, we examined the antigen-specific adaptive immune response. We isolated primary cells from either spleen or cervical and axillary lymph nodes of WT and HLA mice at 28 DPI after immunizations with either CFA or CFA/α-syn$_{32-46}$ (**Figure S5A**). Cells were stimulated *in vitro* for 48 hours with either the peptide, PBS or Concanavalin A (ConA), as respective negative and positive controls. We then measured IFNγ and IL-17A levels, secreted by T_H1 and T_H17 lymphocytes, which are also elevated in the blood of PD patients (Sommer et al., 2018; Yang et al., 2014). α-Syn$_{32-46}$ and ConA induced IFNγ and IL-17A secretion from WT splenocytes and lymph cells, but had no effect on cells from

CFA and CFA/α-syn$_{32-46}$- immunized HLA mice (p= 0.0691; **Figure S5B, C, G, H**; data not shown). The low levels of IFNγ in CFA/α-syn$_{32-46}$ HLA splenocytes were released primarily by CD4$^-$ CD8$^-$ cells (p<0.0001), in contrast to the response of WT splenocytes after *in vitro* re-stimulation with α-syn$_{32-46}$, which was largely driven by CD4$^+$ T cells (p= 0.0160; **Figure S5D-F**). Thus, CD4$^+$ T cells secreting IFNγ and IL-17A were not present in the spleens or lymph nodes in CFA/α-syn$_{32-46}$-immunized HLA mice at 28 DPI, a response consistent with either release from these organs, or loss due to cell death after *in vitro* re-stimulation.

To determine if α-syn$_{32-46}$ immunizations induced a humoral immune response in HLA mice, we assessed the levels of antibodies that recognize α-syn$_{32-46}$ peptide from blood at 28 DPI. In both WT and HLA mouse strains, CFA/α-syn$_{32-46}$ immunization produced high levels of antigen-specific antibodies (**Figure S6I**). Thus, CFA/α-syn$_{32-46}$ immunizations in DRB1*15:01 HLA mice trigger an immune response consistent with bulk RNAseq data; however, the α-syn$_{32-46}$ – specific T cells have likely left the peripheral lymphoid organs and are redistributed to other organs, potentially the ENS.

CD4$^+$ T$_H$1 / T$_H$17 cells adopt a tissue resident memory gene signature in the ileum of CFA/α-syn$_{32-46}$ immunized HLA mice typically found in inflamed mucosal barriers

To determine which immune cell types are responsible for the upregulated pathways identified by bulk RNAseq of the ileum in CFA/α-syn$_{32-46}$, -immunized HLA mice, in particular the adaptive immune response, we performed scRNAseq and analysis on fluorescence-activated cell sorted (FACS) intestinal CD45$^+$ immune cells after dissociation of the small intestine from sick CFA/α-syn$_{32-46}$, CFA-immunized, or PBS-injected HLA mice at 21 DPI (**Figure 5A; Table S2A**). We performed normalization, feature selection, and non-linear dimensional reduction of the raw gene expression data after removal of ribosomal (*Rps*/*l*-) and mitochondrial (*Mt*-) genes associated with technical artifacts from enzymatic

dissociation. After quality control and filtering, 5430 cells from PBS-injected, 9826 cells from CFA, and 12642 cells from CFA/α-syn$_{32-46}$ -immunized HLA mice were used for downstream analysis (**Table S2A**). We used Harmony batch correction to integrate scRNAseq data from three batches (Korsunsky et al., 2019), and identified 27 unique cell clusters from the three conditions using the non-linear dimensional reduction technique UMAP (**Figures 5D, S6A**). The UMAP analysis revealed large populations of lamina propria T cell subtypes, intraepithelial lymphocytes (IELs) and plasma cells, and smaller populations of myeloid cells, innate lymphoid cells, and memory B cells isolated from the gut in each condition (**Figure 5D, E; Table S2B**).

Since CFA/α-syn$_{32-46}$ immunization in HLA mice triggered constipation and enteric neuronal loss, we postulated that α-syn-specific CD4$^+$ T cells may home to the gut, as they were not present in lymphoid tissue (**Figure S5**). To examine transcriptome changes in CD4$^+$ T cell subtypes after α-syn$_{32-46}$ immunization, we separated CD4$^+$ T$_H$1 and T$_H$17 cell clusters from the CD45$^+$ single cell dataset and performed differential gene expression analysis among three conditions **(Figure 5F, H, K)**. T$_H$1, and to a lesser extent T$_H$17, cells isolated from CFA/α-syn$_{32-46}$-immunized HLA mice upregulated a gene signature reminiscent of CD4$^+$ tissue resident memory cells (T$_{RM}$; high levels for *Crem*, *Vps37b*, *Ramp3*, *Ifngr1* and *Tnfrsf4*; **Figure 5G, I, J, L, M)**; this signature has been identified recently in the murine colon and the murine lung following viral infection (Andreatta et al., 2022; Miragaia et al., 2019; Swarnalekha et al., 2021; Tanemoto et al., 2022). T$_H$1 cells from CFA/α-syn$_{32-46}$ immunization also upregulated *Fosl2* expression **(Figure 5J)**, a gene essential for acquisition of an T$_{RM}$ identity [reviewed in (Yenyuwadee et al., 2022)]. Both T$_H$1/T$_H$17 populations upregulated pro-survival memory genes [e.g., *Bcl2* and *Il7r* (**Figure 5J, M)]**; however, *Id3*, a marker of CD4$^+$ memory T$_H$1 cells (Shaw et al., 2022) was absent from the T$_H$1 population in CFA/α-syn$_{32-46}$-immunized HLA mice, suggesting that they were not typical memory cells. We re-clustered T$_H$1 and T$_H$17 cells to identify putative subpopulations with distinct T$_{RM}$ signatures **(Figure 5H, K)**. There was an enrichment for T$_{RM}$ gene signatures in subcluster 2 of T$_H$1

population, which was over-represented by cells from the CFA/α-syn$_{32-46}$-immunized HLA mice **(Figure 5H, I; Table S2B)**. In contrast, the T_{RM} gene signature was more dispersed among the five T_H17 subclusters **(Figure 5K, L)**. The T_H1/T_H17 cell effector genes and cytokines (*Cd69*, *Ifng* and *Il22*) were also significantly downregulated in T_H17 cells from CFA/α-syn$_{32-46}$-immunized mice **(Figure 5M),** whereas additional T_{RM} genes such as *Rgs2* (Amezcua Vesely et al., 2019; Li et al., 2016) and *Samsn1* (Gaublomme et al., 2015; Miragaia et al., 2019) were upregulated in T_H17 cells from CFA/α-syn$_{32-46}$ HLA mice **(Figure 5M)**. Gene-set enrichment analysis (GSEA) of T_H1 and T_H17 cells did not reveal significant GO terms associated with genes enriched from CFA/α-syn$_{32-46}$-immunization in HLA mice. Overall, these results demonstrate that CFA/α-syn$_{32-46}$ immunizations in HLA mice triggered transcriptome shifts in $CD4^+$ T_H1 / T_H17 cells consistent with a tissue resident memory phenotype, similar to the signature found in antigen-experienced T_{RM} cells at mucosal barriers following infection or chronic inflammation. The transcriptome identity shift provides an explanation of why T_H1 / T_H17 cells were not found in peripheral lymphoid organs in CFA/α-syn$_{32-46}$-immunized HLA mice (**Figure S5**).

Two populations of IELs (IEL 1, induced IEL) were predominately derived from the CFA/α-syn$_{32-46}$ immunized HLA mice (>45% of the cluster), even after correcting for cell numbers from other conditions **(Figure 5E; S6C, D, F; Table S2B).** These two clusters were characterized by a high expression of effector T cell markers and cytokines (*Itgae*, *Cd69*, *Gzma*, *Gzmb*, *Id2*), but low expression of memory genes (*Id3*, *Tcf7*, *Xcl1*) (**Figure S6F**). The third population of IELs (IEL 2) expressed high levels of $CD8^+$ T cell memory identity (*Id3*, *Tcf7*, *Xcl1*), but lacked expression of effector cytokines (*Ifng*, *Gzma*, and *Gzmb*) (**Figure S6F**). In contrast to the $CD8\alpha^+$ IEL 1 cluster, the $CD8\alpha\beta^+$ induced IEL cluster is likely derived from antigen-experienced $CD8^+$ T cells which home to intestinal epithelium following activation [reviewed in (Cheroutre et al., 2011)] . Differential gene expression analysis of induced IELs among three conditions revealed upregulation of T_{RM}-associated genes (e.g., *Nr4a1*, *Rgs2*, and *Vps37b*) in

CFA/α-syn$_{32-46}$ immunized HLA mice (**Figure S6E, F**). Based on this unique gene signature, the induced IELs are likely an effector-like antigen-experienced CD8αβ$^+$ IEL population (Wang et al., 2023) highly enriched in CFA/α-syn$_{32-46}$ immunized HLA mice. Granulocytes, composed of CCR3$^+$ eosinophils and CXCR2$^+$ neutrophils, were predominantly derived from CFA-immunized HLA mice **(Figure S6G).** Differential gene expression analysis revealed upregulated genes associated with granules (*Lcn2*, *Chil3*) and the type 1 interferon response (*Ifitm1*, *Ifitm2*, *Ifitm3*, *Ifitm6*, *Irf1*, *Ifnar2*) in CFA/α-syn$_{32-46}$- compared with CFA-immunized HLA mice **(Figure S6J, K)**. GSEA confirmed enrichment of genes for: a) defense response to bacterium (GO: 0042742); b) response to interferon beta (GO: 0035456); and c) humoral immune response (GO: 0006959) **(Figure S6I)**. Overall, the scRNAseq analysis of immune cells shows that the immune response in the gut at peak constipation (21 DPI; **Figure 5A-C**) was driven not only by CD4$^+$ T cells, but also CD8αβ$^+$ effector IEL cells and granulocytes, that likely contribute to disease outcomes.

CD4$^+$ T cells are partially responsible for the ENS dopaminergic neuron damage

Since CD4$^+$ T cells and CD8αβ$^+$ effector IEL cells drive immune responses in the gut of CFA/α-syn$_{32-46}$ immunized HLA mice, we depleted either CD4$^+$ or CD8$^+$ T cells with anti-CD4, anti-CD8, or isotype control antibodies administered before and at weekly intervals after α-syn$_{32-46}$ immunization to determine which cells are critical for inflammation, neurodegeneration and constipation (**Figure 6A**). Flow cytometry analysis of peripheral blood showed that the appropriate antibody treatments depleted CD4$^+$ and CD8$^+$ T cell types in mice (**Figure 6B**).

A high proportion (~64%) of CFA/α-syn$_{32-46}$ immunized HLA mice treated with the IgG isotype control did not survive to 28 DPI, while nearly all CD4$^+$- or CD8$^+$- depleted CFA/α-syn$_{32-46}$- immunized HLA mice survived until sacrifice (**Figure 6C, D**). Weight monitoring revealed no significant difference

in weight loss across all treatment groups (**Figure 6E**). All groups showed similar GI transit times (**Figure 6F**) and there was no significant difference in macrophages in either myenteric or submucosal plexuses (**Figure 6P, Q**). Importantly, histopathological analysis revealed a rescue of TH^+ neurons in the submucosal plexus of $CD4^+$-depleted CFA/α-syn_{32-46} HLA mice, but no rescue by the depletion of $CD8^+$ T cells (**Figure 6G-K**). Interestingly the neuronal loss appeared to be specific to TH^+ cells, as other ENS neurons remained unchanged across all treatment groups. Thus, $CD4^+$ T cells may be in part responsible for inducing TH^+ cell damage and loss after CFA/α-syn_{32-46}-immunizations in HLA mice, but additional factors like $CD8\alpha\beta^+$ effector IEL cells, or granulocytes may contribute to other disease phenotypes such as constipation and weight loss.

DISCUSSION

PD is a multifactorial disease and dysregulation of the immune response targeting α-syn has been strongly implicated as a potential driver of pathogenesis, at least in a subset of PD patients during the first decade after diagnosis (Garretti et al., 2019; Lindestam Arlehamn et al., 2020; Sulzer et al., 2017). Our previous studies have shown that $CD4^+$ T cells that respond prominently to two regions of the α-syn protein are found in the blood of PD patients (Sulzer et al., 2017). Although the immune response to the α-syn_{32-46} region is restricted to patients carrying a specific HLA haplotype [B*07:02 C*07:02 DRB5*01 DRB1*15:01 DQA1*01:02 DQB1*06:02] (Sulzer et al., 2017), how these interactions trigger PD pathogenesis is unknown.

Using an active immunization approach in mice similar to induction of the EAE mouse model for human MS (Lengfeld et al., 2017; Lutz et al., 2017), we find that α-syn_{32-46} peptide immunizations in mice in which their native MHC class II allele was substituted by the human HLA DRB1*15:01 allele recapitulate multiple aspects of the immune response detected in PD patients. These include loss of ENS neurons, a progressive decrease in dopaminergic neuronal processes, weight loss and constipation,

features reminiscent of clinical gastroenterological deficits reported in PD patients twenty years prior to disease onset (Khoo et al., 2013) (**Figure 7**). Some of these disease phenotypes (e.g., progressive decrease in dopaminergic neurons) require, at least in part, $CD4^+$ T cells (**Figure 6**), although the mechanisms by which $CD4^+$ T cells mediate them are unclear. Our findings confirm previous hypotheses that α-syn_{32-46} antigen / HLA-DRB1*15:01 interactions underlie some of the prodromal stages of PD manifested by prominent gut inflammation and $CD4^+$ T cell-driven loss of enteric neurons.

While the immunizations generated a strong antibody response to α-syn_{32-46} in both WT and HLA mice, we found that T_H1, T_H17 and $CD8^+$ T cells that responded to the peptide were retained in spleen and axillary lymph nodes only in WT mice. Strikingly, α-syn_{32-46} - specific $CD4^+$ T cells were absent in immune organs in CFA/α-syn_{32-46} - immunized HLA mice (**Figure S5**). This observation is consistent with effective homing of these $CD4^+$ T cells from dedicated immune organs to the gut (McLachlan and Jenkins, 2007), where they are likely responsible for gastrointestinal inflammation, loss of ENS neurons and constipation (**Figure 7**). Single cell RNA sequencing of intestinal immune cells confirmed the presence of $CD4^+$ T_H1 and T_H17 lymphocytes in the gut of CFA/α-syn_{32-46} peptide immunized mice, where these cells adopted a transcriptome signature characteristic of antigen-experienced tissue resident memory cells found in mucosal barriers during infection and chronic inflammation, including IBD [reviewed in (Lange et al., 2022; Lyu et al., 2022)] (**Figure 5G-M**).

In our humanized mouse model, constipation, a GI symptom present in the majority of PD patients, specifically required the combination of α-syn_{32-46} and the HLA DRB1*15:01 allele. While other PD mouse models have reported constipation (Metzger and Emborg, 2019; Sampson et al., 2016), our study demonstrates that a specific combination of an α-syn-derived epitope and an HLA allele can drive gut pathology and dysmotility. This pathology is characterized by activation of innate and adaptive immune gene signatures (**Figure 5B, C**), which is followed initially by a loss of $ANNA1^+$ enteric neurons

in the submucosal plexus at 28DPI, and subsequently by a progressive reduction in TH^+ neuronal processes and intensity between 28-42 DPI in CFA/α-syn_{32-46} HLA mice (**Figures 3, 4, 7**).

Depletion experiments of $CD4^+$ and $CD8^+$ T cell suggest that $CD4^+$ T cells are critical drivers of dopaminergic neuron damage and loss in the gut, and are consistent with other studies implicating $CD4^+$ T cells in neuronal damage in other PD mouse models (Brochard et al., 2009; Williams et al., 2021). The timing of the enteric features in this model are consistent with a robust interferon response gene signature revealed by bulk RNAseq (**Figure 5B, C**). While we find that $CD4^+$ T cells promote enteric neuron loss, the relationship between $CD4^+$ T cell-mediated neuronal loss and interferon response requires further investigation. The interferon response at 21 DPI may reflect dying enteric neurons with an increase in extracellular nucleic acids. Type 1 interferon response have been suggested to play a non-classical role in neurodegeneration, including in the MPTP mouse model for Parkinson's disease (Main et al., 2016).

Our single cell RNA sequencing has identified a population of $CD4^+$ T_{RM} cells present in the gut of sick CFA/α-syn_{32-46}-immunized HLA mice at 21DPI. In human IBD, $CD4^+$ $CD69^+$ $CD103^+$ T_{RM} cells are proposed to accumulate and regulate intestinal inflammation (Lyu et al., 2022; Zundler et al., 2019). A similar $CD4^+$ T_{RM} population ($CD161^+$ $CCR5^+$) produces proinflammatory cytokines in Crohn's disease (Yokoi et al., 2023). Populations of $CD103^-$ $CD4^+$ T_{RM} cells similar to those identified in our scRNAseq results have been shown to expand following antigen exposure. For example, *Aspergilus fumigatus* generates $CD103^-$ $CD4^+$ T_{RM} cells in the murine lung, which produce proinflammatory cytokines and contribute to fibrosis [reviewed in (Hirahara et al., 2021)]. In addition to $CD4^+$ T_{RM} cells, $CD8^+$ $CD103^-$ T_{RM} cells in the intestine give rise to $CD8^+$ $CD103^+$ T_{RM} cells that respond to secondary infections (Fung et al., 2022; von Hoesslin et al., 2022). The identification of $CD4^+$ T_{RM} cells in the gut of CFA/α-syn_{32-46}-immunized HLA mice at 21 DPI, coupled with the critical role that these cells play in chronic inflammation, suggest that they may play a critical role to drive ENS pathology in the gut.

The overrepresentation of induced IELs and granulocytes from CFA/α-syn$_{32-46}$ -immunized HLA mice suggests that the expansion from antigen exposure may not be limited to CD4^{+} T cells. These additional immune cells may play important roles in the gut pathology following CFA/α-syn$_{32-46}$ immunizations, although this is difficult to ascertain with our small sample size. Other immune cell types are likely involved in the constipation phenotype, and future studies with enrichment of specific immune subtypes could provide additional insights into their role in disease pathogenesis. Granulocytes isolated from CFA/α-syn$_{32-46}$-immunized mice displayed an anti-bacterial phenotype compared to the CFA-immunized mice, since the inducer of anti-bacterial inflammation lipocalin-2 (*Lcn2*) was highly upregulated in this population. *Lcn2* is highly expressed in intestinal inflammation, including IBD [Reviewed in (Moschen et al., 2017)]. Such robust antimicrobial responses in our immunization model may suggest the presence of a leaky gut, which could also contribute to the constipation phenotype. The interferon responses that were highly upregulated from bulk RNA sequencing are largely absent from the single cell dataset, with the exception of granulocytes from CFA/α-syn$_{32-46}$-immunized mice **(Figure S6I, K; Table S2)**. It is likely that other cells in the intestine, such as epithelial cells, may produce the majority of the transcriptional responses detected by bulk RNA sequencing of the ileum. These collective bulk and single cell RNA sequencing data support the model that HLA-α-syn$_{32-46}$ interactions drive innate and adaptive immune responses in the gut that underlie the pathology, and α-syn-specific CD4^{+} T cells are critical, at least in part, to drive the enteric features of prodromal PD.

The mechanisms by which CD4^{+} T cells mediate enteric neuronal loss remain unclear, although their roles have been confirmed in Parkinson's rodent models with prominent CNS damage (Harms et al., 2021; Williams et al., 2021). The immune-dependent loss of dopaminergic neurites may be transient, and could be related to a temporary loss of the TH^{+} marker expression (Harvey et al., 2000; Hotchkiss and Gibb, 1980; Soriano et al., 1997), as has been shown in other peripheral neurons (Coulombe and Bronner-

Fraser, 1986; Wolinsky and Patterson, 1983), although it has also been reported that newborn dopamine neurons may appear in the adult small intestine in response to their death (Kulkarni et al., 2017).

While constipation is strongly associated with prodromal PD, there is little analysis of the inflammatory state or neurodegeneration associated with that condition. The density of enteric neurons in the small intestine is reported to correlate with clinical features of dysmotility (Boschetti et al., 2019). Although dopamine has been shown to be essential for normal gastrointestinal motility in rodents (Li et al., 2006), some biopsy studies of the gut report no difference in dopaminergic neurons between PD patients and healthy controls (Annerino et al., 2012; Corbille et al., 2014; Lebouvier et al., 2010), while others report changes in dopamine in inflammatory bowel disease (Kurnik-Lucka et al., 2021). These analyses are of the colon, and enteric neurons are irregularly distributed across the two plexuses of the 25 feet-long human adult bowel (Rao and Gershon, 2016), making it challenging to thoroughly analyze such specimens. Our study examines up to 1 mm^2 of myenteric and submucosal plexus of the ileum per mouse at confocal resolution, offering a broad analysis of this enteric region. Importantly, our mouse model examines gut responses to two acute immunizations with a self-antigen, in contrast to chronic antigen exposure present in PD; it is possible that ENS symptoms in PD, including constipation, might wax and wane depending on the presence of specific epitopes, particularly α-syn$_{32-46}$ or phosphorylated S129.

A transient CNS entry of peripheral T cells that recognize a mitochondria-derived antigen associated with intestinal inflammation was reported to drive SN dopamine axonal loss in *Pink1*-deficient mice (Matheoud et al., 2019). In contrast, we observed no CNS symptoms ($CD3^+$ T cell infiltrates, neuroinflammation or loss of dopaminergic neurons) in the α-syn$_{32-46}$ / HLA DRB1*15:01 mouse model, consistent with reports that ENS symptoms appear decades prior to CNS symptoms in PD patients. The lack of CNS damage in the α-syn$_{32-46}$ / HLA DRB1*15:01 model suggests that a “second hit” is required to target α-syn-specific T cells into the CNS, followed by neuroinflammation and loss of central

dopaminergic neurons. This could be due to the transient, rather than chronic, exposure to the α-syn epitope (two rounds of immunizations in mice in contrast to chronic exposure over decades in PD patients), or insufficient HLA-associated presentation of the α-syn peptide by antigen presenting cells in the brain, which may in turn result from disease-associated altered degradation pathways that produce neoepitopes.

In conclusion, we have shown that α-syn autoimmunity is sufficient to induce constipation and gut pathology with loss of enteric neurons that can elicit prodromal symptoms of PD. The demonstration that a restrictive HLA allele in combination with an α-syn-derived antigen leads to prodromal PD-like symptoms suggests that autoimmune responses to α-syn-derived epitopes may play an early role in PD pathogenesis.

ACKNOWLEDGEMENTS

We thank Michael D. Gershon, Alcmene Chalazonitis-Green, and Wanda Setlik (CUIMC) for guidance with enteric dissections, staining, and behavior experiments, and particularly with the analysis of neuronal number and area in the flat mount ileum preparations; Ilir Agalliu (AECOM) for his advice with advanced statistical analysis; Peter Sims (CUIMC) for his guidance with the analysis of scRNAseq data; Ori Lieberman, Michael Post, Charlotte Wayne, Madeline Edwards, Megan Sykes, Ai Yamamoto, and Wassim Elyaman (CUIMC) for suggestions with various experiments throughout this study. This research was funded in part by Aligning Science Across Parkinson's [#0375] through the Michael J. Fox Foundation for Parkinson's Research (MJFF). For the purpose of open access, the authors have applied a CC BY public copyright license to all Author Accepted Manuscripts arising from this submission. D.S and E.K are also supported by NIH/NINDS (R01 NS095435) and the JPB Foundation. T.C., S.S., and D.A., are also supported by grants from the NIH/NIMH (R01 MH112849), NIH/NIE (R01 EY033994), the National MS Society (RG-1901-33218). D.A., and T.C., are partially supported by unrestricted gifts

from the Newport Equities LLC, the Walz family and PANDAS Network to the Department of Neurology, CUIMC.

AUTHOR CONTRIBUTIONS

F.G., D.A., A.S., and D.S., conceived the project; F.G., C.M., N.S., S.S., S.W.K., T.C., E.K. and D.A. performed the experiments and analyses, F.G., C.M., T.C. A.S., D.A., and D.S. wrote and edited the manuscript, and F.G. and C.M. prepared figures and figure legends.

COMPETING INTERESTS

The authors declare that the research was conducted without any commercial or financial relationships that can be construed as potential conflicts of interest.

STAR METHODS

RESOURCE AVAILABILITY

Lead Contact

Further information and requests for resources and reagents should be directed to and will be fulfilled by the lead contact, David Sulzer (ds43@cumc.columbia.edu).

Materials availability

This study did not generate new unique reagents.

Data and code availability

Data

Microscopy reported in this paper will be shared by the lead contact upon request. RNA-sequencing data will be made available on the NCBI Gene Expression Omnibus (GEO) database.

Code

This paper does not report original code.

Section 3

Any additional information required to reanalyze the data reported in this paper is available from the lead contact upon request.

EXPERIMENTAL MODEL AND SUBJECT DETAILS

Mice

All experimental procedures were approved by the Institutional Animal Care and Use Committee (IACUC) at Columbia University Irving Medical Center (CUIMC). Generation of transgenic mice expressing the *HLA DRB1*15:01* α and β chains in the C57BL/6 background have been previously described (Krogman et al., 2017). Wild-type C57BL/6J were obtained from the Jackson Laboratory (Bar Harbor, ME). The HLA transgenic mice lacking mouse MHC-II were backcrossed to the C57BL/6J strain (Jackson Laboratory; Bar Harbor, ME) for more than 8 generations. All mice were bred within the barrier facility of CUIMC and group housed, fed regular chow. Both female and male mice were used in this study in equal numbers at the ages described in the text.

METHOD DETAILS

Immunizations

8- to 12-week-old male and female mice were immunized subcutaneously with a 100 μl emulsion of 100 μg α-syn$_{32-46}$ peptide (A&A peptides; San Diego, CA) dissolved in PBS with Complete Freund Adjuvant (CFA) containing 200 μg of *M. tuberculosis* H37Ra (BD Difco Adjuvant, Fisher Scientific, Cat #DF0638-60-7; Waltham, MA). The day of immunization was designated as day 0. Mice received a boost

with the same immunization dose two weeks later. Mice received intravenous injections of 400 ng of *B. pertussis* toxin (List Biological Laboratories, Cat #181; Campbell, CA) 14- and 16-days post-initial immunization (day 0 and 2 post boost). Control animals received *B. pertussis* toxin and emulsion containing PBS/CFA without the protein or the α-syn peptide. Additional control mice received subcutaneous injections of PBS only. Mice were monitored for their weight, food and fluid intake and neurological deficits and their weights were recorded daily. Mice were classified as sick if they displayed 12% reduction from 0 DPI weight and/or hunched posture with ruffled and ungroomed fur.

Gut dissections

Mice were perfused with PBS and segments of the ileum were collected in PBS. The contents were flushed out with PBS and the preparations were cut open along the mesenteric border. The flat tissue was stretched tautly and pinned flat on Sylgard (Sylgard™ 184, Dow Corning, Cat #240-4019862; Midland, MI) with the mucosa surface facing up. Specimens were fixed for one hour at room temperature 4% paraformaldehyde and washed three times with PBS for a total of 30 min. The mucosa and submucosal plexus were removed from specimen by microdissection. Then, the mucosal was separated from the submucosal layer. The longitudinal muscles were dissected from the specimen to reveal the myenteric plexus. The submucosal and myenteric plexuses were collected and store in PBS at 4°C until immunofluorescence staining.

Intestinal flat mount immunofluorescence staining and analysis

Staining

For immunofluorescence analysis, intestinal flat mounts were blocked and permeabilized for 1 hour at room temperature with 10% normal donkey serum (Jackson Immunoresearch, Cat #017-000-121; West Grove, PA) and 1% Triton-X in PBS. Intestinal flat mounts were then incubated overnight at room temperature with primary antibodies in 10% normal donkey serum, 1% Triton-X in PBS. Sections were

stained with antibodies against tyrosine hydroxylase (TH) (1:500, Millipore-Sigma, Cat # AB152; Burlington, MA) and CD3 (1:400, Bio-Rad Laboratories, Cat #MCA2690; Hercules, CA), ANNA1 (1:32,000; kind gift by the Gershon laboratory (Margolis et al., 2016)), Iba1 (1:500, WAKO, Cat # 019-19741; Richmond, VA), CD68 (1:1000, Abcam, Cat # ab53444; Waltham, MA). Secondary antibodies with the appropriate conjugated fluorophores were purchased from Invitrogen. Images were acquired with an LSM700 confocal microscope and processed with Fiji software (ImageJ, NIH; Bethesda, MD).

Acquisition

For enteric neuron imaging, both the myenteric (MP) and submucosal plexus (SP) for each mouse were analyzed. Within each plexus of each animal, 2-3, 2x2 tile z-stack 640.17x 640.17 µm confocal images at 20x magnification were acquired. This totaled to over 1 mm^2 of flat-mount enteric tissue imaged and analyzed per mouse. For imaging macrophages, both the MP and SP were analyzed for each animal. Within each plexus of each animal, 2-3, z-stack 390.09 x 390.09 µm confocal images at 20x magnification were acquired.

Analysis

The investigator who analyzed the images was blinded to each condition. The number of $ANNA1^+$, TH^+ cells, and $IBA1^+$ cells were counted for each image within each layer. Within the SP, the TH^+ signal was thresholded and the area and MFI of the thresholded TH^+ signal was analyzed for mean fluorescent intensity and size of area. The thresholding was consistent across each image, animal, and condition within each experiment. Within each animal, the number of $ANNA1^+$, TH^+ cells, and $IBA1^+$ cells across all images were summed and divided by acquisition area. Within each experiment, the cell numbers were normalized to CFA only.

Total GI transit

Carmine red, which cannot be absorbed from the lumen of the gut, was used to study total gastrointestinal (GI) transit time (Kimball et al., 2005). A solution of carmine red (300 µl; 6%; Sigma-Aldrich, Cat #C1022; St Louis, MO) suspended in 0.5% methylcellulose (Sigma-Aldrich, Cat #M0512; St Louis, MO) was administered by gavage through a 21-gauge round-tip feeding needle. The time at which gavage took place was recorded as T_0. After gavage, fecal pellets were monitored at 10 min intervals for the presence of carmine red. Total GI transit time was considered as the interval between T_0 and the time of first observance of carmine red in the stool.

Bulk RNA sequencing of the ileum

Ileum samples were incubated in TRIzol reagent (Thermo Fisher Scientific, Cat #15596026; Waltham, MA) and stored at -80 □C. Total RNA was extracted and assessed for quality utilizing Agilent bioanalyzer for quantitation of RNA/DNA/protein (CUIMC Molecular Pathology Core). cDNA library preparation and RNA sequencing were performed by the CUIMC Genome Center. mRNAs were enriched from total RNA samples with poly-A pull-down, then processed with library construction using Illumina TruSeq chemistry. Libraries were then sequenced using Illumina NovaSeq6000 at CUIMC Genome Center. Samples were multiplexed in each lane, which yielded targeted number of paired-end 100bp reads for each sample. RTA (Illumina) for base calling and bcl2fastq2 (version 2.19) were used for converting BCL to fastq format, coupled with adaptor trimming. A pseudoalignment was performed to a kallisto index created from transcriptomes (GRCm38) using kallisto (0.44.0). Differentially expressed genes under various conditions were tested using DESeq2R packages designed to test differential expression between two experimental groups from RNA-seq counts data. Genes were considered differentially expressed if they had an adjusted p-value <0.05 and a $\log_2$fold change below or above 0.5. The differential expression was normalized for each gene.

<u>Single cell RNA sequencing of the ileum</u>

Isolation of intestinal immune cells

The methods used for isolation of intestinal immune cells were adapted from Ivanov et al. (Ivanov et al., 2006). Briefly, mice were perfused with PBS and the small intestine was removed. Peyer's patches were dissected from the small intestines, and the intestine was cut open longitudinally. Intestinal contents were removed by scraping along the tissue with rounded forceps, followed by 5-6 washes with cold PBS. The intestine was cut into large fragments, then placed in 5-10 mL of cell dissociation solution (5mM EDTA, 10mM HEPES, in HBSS supplemented with 2.5% FBS) and incubated for 10 minutes at 37°C rotating at 100 rpm. After 10 minutes, the solution was vortexed for 25 seconds, then the supernatant was collected and discarded using a wire mesh to collect the tissue. The tissue was incubated again in fresh cell dissociation solution, then the additional supernatant was discarded as previously described. The tissue fragments were rinsed in HBSS then cut into small pieces (~1 mm^2). The small fragments were incubated in three 20-minute intervals at 37 C with slow rotation in 5 mL of digestion solution (0.5 mg/mL collagenase D (Roche, Cat# 11088858001; Mannheim, Germany), 0.5 U/mL Dispase (Stem Cell Technologies, Cat# 07913; Vancouver, Canada), 0.5 mg/mL DNase I (Roche, Cat# 10104159001; Mannheim, Germany), in RPMI supplemented with 5% FBS). After each 20-minute digestion period, the solution was vortexed for 30 seconds, then the supernatant was collected by filtering through a 100 µm strainer. The remaining tissue fragments were placed in new digestion solution for subsequent washes. All supernatants were combined then resuspended with 10 mL of 40% Percoll (Sigma-Aldrich, Cat# GE17-0891-01; St. Louis, MO) in RPMI with 10% FBS. The resuspended cells were gently added on top of 5 mL 80% Percoll in RPMI with 10% FBS in a 15 mL conical tube. The tubes were centrifuged at 2500 rpm for 20 minutes without brake. The cell layer at the interface between 40% and 80% Percoll was collected, diluted in RPMI with 10% FBS. The cells were pelleted, then resuspended in FACS buffer, consisting of 1% bovine serum albumin (Sigma-Aldrich, Cat# A9647-100G; St. Louis, MO) in PBS.

FACS

The cells isolated from the small intestine were resuspended with 400 µl Fc block (BD Biosciences, Cat# 553142; Franklin Lakes, NJ), 1:200 in FACS buffer, and incubated for 20 minutes on ice. The cells were washed in 500 µl FACS buffer, pelleted at 1500 rpm for 2 minutes, then resuspended in 600 µl of FACS buffer with 1:100 CD45 BUV395 antibody (BD Biosciences, Cat# 564279; Franklin Lakes, NJ) and incubated on ice for 30 minutes. After 30 minutes, the cells were washed in 500 µl FACS buffer, then resuspended in 500 µl of FACS buffer containing propidium iodide (BioLegend, Cat# 421301; San Diego, CA) at 1:10,000. Viable, $CD45^+$ cells were sorted by the Sony MA900 Multi-Application Cell Sorter.

Analysis

The isolated $CD45^+$ intestinal immune cells were processed by the Single Cell Analysis Core at Columbia University using the TruSeq Stranded mRNA Library Prep Kit (Illumina) and sequenced on an Illumina NovSeq 6000 platform. The Single Cell Analysis Core used 10X Cell Ranger analysis software (version 5.0.1) to process fastq files using "cellranger count" for each sample individually with default parameters producing an alignment of reads to the mm10-2020-A transcriptome. The gene-cell matrices were processed, including normalization, scaling, selection of features, linear dimensional analysis, and clustering, using the Seurat package v4.0.0 in R Studio (Hao et al., 2021). For quality control, cells with fewer than 15% mitochondrial reads and UMI counts between 1000 and 50000 were kept for downstream analysis. Ribosome (*Rps*/*l*-) and mitochondria (*Mt*-) associated genes were regressed from the dataset to remove effects of technical artifacts of the cell dissociation process. Batch correction was performed with the Harmony package (Korsunsky et al., 2019). UMAP clusters were manually annotated by assessment of differentially expressed features using the FindMarkers function in the Seurat package **(Figure S6B; Table S2C)**.

T cell depletions

Mice were injected interperitoneally with 250 μg of Ultra-LEAF Purified anti-mouse CD4 or Rat IgG2b isotype control antibodies (Biolegend, Cat #100457 and Cat #400644; San Diego, CA) 3 and 1 days prior to immunization. After immunization, mice were injected with 250 ug of antibody weekly. Cell depletion was assessed via flow cytometry. For depletion of $CD8^+$ T cells, mice were injected interperitoneally with 250 μg of Ultra-LEAF Purified $CD8^+$ or Rat IgG2b isotype control antibodies (Biolegend Cat # 100746 and Cat #400644; San Diego, CA) 2 days prior to immunization. After immunization, mice were injected with 250 ug of each antibody 9- and 19-days post immunization, then cell depletion was determined via flow cytometry.

QUANTIFICATION AND STATISTICAL ANALYSIS

Fiji software (ImageJ, NIH; Bethesda, MD) was utilized for the quantitation of immunofluorescence images. Statistical analysis was performed using GraphPad Prism software version 8.0 (Graphpad Software Inc; San Diego, CA). For enteric immunofluorescence analysis, we compared $ANNA1^+$ and TH^+ cell density and TH^+ area and MFI among 3 immunization groups: PBS, CFA only, or CFA/α-syn_{32-46} using one way analysis of variance (ANOVA). In addition, we used Scheffe method for multiple comparisons given that 3 groups had unequal sample size. We then fitted a general linear regression with immunization group as exposure and adjusted for variability from two different raters (FG vs. CM). All tests were 2-sided with significant level set at $p<0.05$. For all other analyses, unpaired t test was used to compare the differences between two groups in studies. One-way and two-way ANOVA followed by Bonferroni post hoc tests were performed to compare the differences among groups. Differences between groups were presented as the mean ± SEM or SD as noted in the figure legends. The sample size (n) for each experiment is indicated in figure legends and the Results section. All tests were two sided and p values < 0.05 were considered to be statistically significant.

KEY RESOURCES TABLE

REAGENT or RESOURCE	SOURCE	IDENTIFIER
Antibodies		
Anti-tyrosine hydroxylase antibody	Millipore	Cat #AB152, RRID:AB_390204
Hamster anti mouse CD3 antibody	Bio-Rad	Cat #MCA2690, RRID:AB_905951
ANNA1	Michael Gershon, CUIMC	(Margolis et al., 2016)
Anti Iba1	FUJIFILM Wako Shibayagi	Cat #019-19741, RRID:AB_839504
CD68 antibody [FA-11]	Abcam	Cat #ab53444, RRID:AB_869007
Ultra-LEAF™ Purified anti-mouse CD4 Antibody	BioLegend	Cat #100457
Ultra-LEAF™ Purified Rat IgG2b isotype control Antibody	BioLegend	Cat #400644
Ultra-LEAF™ Purified anti-mouse CD8 Antibody	BioLegend	Cat # 100746
Fixable viability dye eFluor 780	eBiosciences	Cat #65-0865
Rat Anti-Mouse CD3 Molecular Complex Monoclonal Antibody, PerCP-Cy5.5 Conjugated, Clone 17A2	BD Biosciences	Cat# 560527, RRID:AB_1727463
BV421 Rat anti-mouse CD4	BD Biosciences	Cat# 562891, RRID:AB_2737870
Brilliant Violet 605(TM) anti-mouse CD8a antibody	Biolegend	Cat# 100743, RRID:AB_2561352
APC Rat anti-mouse IFN-g	BD Biosciences	Cat# 554413, RRID:AB_398551
Rat Anti-IL-17 Monoclonal Antibody, Phycoerythrin Conjugated, Clone TC11-18H10.1	BD Biosciences	Cat# 559502, RRID:AB_397256
CD45 Monoclonal Antibody (30-F11), PerCP-Cyanine5.5, eBioscience™	Thermo Fisher Scientific	Cat# 45-0451-80, RRID:AB_906233
Goat Anti-Mouse IgG H&L (HRP) antibody	Abcam	Cat# ab205719, RRID:AB_2755049
Chemicals, peptides, and recombinant proteins		
EndoClear™ human recombinant a-Synuclein protein	AnaSpec	Cat #as-55555
α -syn$_{32-46}$ (KTKEGVLYVGSKTKE)	A&A peptides	Per request
Pertussis Toxin from *B. pertussis*, Lyophilized (Salt-Free)	List Labs	Cat #181
Complete Freund Adjuvant (CFA) containing 200 μg of *M. tuberculosis* H37Ra	BD Difco Adjuvant, Fisher Scientific	Cat #DF0638-60-7
Carmine (powder)	Millipore- Sigma	Cat #C1022
Concanavalin A	Millipore-Sigma	Cat #C2010
Critical commercial assays		

Mouse IFN-gamma DuoSet ELISA	R&D systems	Cat #DY485
Mouse IL-17A DuoSet ELISA	R&D systems	Cat #DY421
Experimental models: Organisms/strains		
Mouse: HLA DRB1*15:01 in C57BL/6J background	This paper, Chella David laboratory (Mayo Clinic)	(Krogman et al., 2017)
Mouse: C57BL/6J	The Jackson Laboratory	Strain #000664
Oligonucleotides		
Primers for hygromycin control. Forward: ctgatcgaaaagttcgacagc, Reverse: gtattgaccgattccttccg	IDT	N/A
Primers for DRalpha. Forward: ccgagctctactgact, Reverse: gacttacttcagtttgtgg	IDT	N/A
Primers for DR2beta. Forward: tcgccgctgcactgtgaag, Reverse: tcctgtggcagcctaagag	IDT	N/A
Software and algorithms		
Fiji	ImageJ	https://imagej.net/software/fiji/
Prism v9.0	GraphPad	https://www.graphpad.com/scientific-software/prism/
DESeq2R	R package	https://bioconductor.org/packages/release/bioc/html/DESeq2.html

REFERENCES

Amezcua Vesely, M.C., Pallis, P., Bielecki, P., Low, J.S., Zhao, J., Harman, C.C.D., Kroehling, L., Jackson, R., Bailis, W., Licona-Limon, P., *et al.* (2019). Effector T(H)17 Cells Give Rise to Long-Lived T(RM) Cells that Are Essential for an Immediate Response against Bacterial Infection. Cell *178*, 1176-1188 e1115.

Andreatta, M., Tjitropranoto, A., Sherman, Z., Kelly, M.C., Ciucci, T., and Carmona, S.J. (2022). A CD4(+) T cell reference map delineates subtype-specific adaptation during acute and chronic viral infections. Elife *11*.

Annerino, D.M., Arshad, S., Taylor, G.M., Adler, C.H., Beach, T.G., and Greene, J.G. (2012). Parkinson's disease is not associated with gastrointestinal myenteric ganglion neuron loss. Acta Neuropathol *124*, 665-680.

Appel-Cresswell, S., Vilarino-Guell, C., Encarnacion, M., Sherman, H., Yu, I., Shah, B., Weir, D., Thompson, C., Szu-Tu, C., Trinh, J., *et al.* (2013). Alpha-synuclein p.H50Q, a novel pathogenic mutation for Parkinson's disease. Mov Disord *28*, 811-813.

Boschetti, E., Malagelada, C., Accarino, A., Malagelada, J.R., Cogliandro, R.F., Gori, A., Bonora, E., Giancola, F., Bianco, F., Tugnoli, V., *et al.* (2019). Enteric neuron density correlates with clinical features of severe gut dysmotility. Am J Physiol Gastrointest Liver Physiol *317*, G793-G801.

Braak, H., Del Tredici, K., Rub, U., de Vos, R.A., Jansen Steur, E.N., and Braak, E. (2003). Staging of brain pathology related to sporadic Parkinson's disease. Neurobiology of aging *24*, 197-211.

Brochard, V., Combadiere, B., Prigent, A., Laouar, Y., Perrin, A., Beray-Berthat, V., Bonduelle, O., Alvarez-Fischer, D., Callebert, J., Launay, J.M., *et al.* (2009). Infiltration of CD4+ lymphocytes into the brain contributes to neurodegeneration in a mouse model of Parkinson disease. J Clin Invest *119*, 182-192.

Cheroutre, H., Lambolez, F., and Mucida, D. (2011). The light and dark sides of intestinal intraepithelial lymphocytes. Nat Rev Immunol *11*, 445-456.

Corbille, A.G., Coron, E., Neunlist, M., Derkinderen, P., and Lebouvier, T. (2014). Appraisal of the dopaminergic and noradrenergic innervation of the submucosal plexus in PD. J Parkinsons Dis *4*, 571-576.

Cossais, F., Schaeffer, E., Heinzel, S., Zimmermann, J., Niesler, B., Roth, R., Rappold, G., Scharf, A., Zorenkov, D., Lange, C., *et al.* (2021). Expression Profiling of Rectal Biopsies Suggests Altered Enteric Neuropathological Traits in Parkinson's Disease Patients. J Parkinsons Dis *11*, 171-176.

Coulombe, J.N., and Bronner-Fraser, M. (1986). Cholinergic neurones acquire adrenergic neurotransmitters when transplanted into an embryo. Nature *324*, 569-572.

Devos, D., Lebouvier, T., Lardeux, B., Biraud, M., Rouaud, T., Pouclet, H., Coron, E., Bruley des Varannes, S., Naveilhan, P., Nguyen, J.M., *et al.* (2013). Colonic inflammation in Parkinson's disease. Neurobiology of disease *50*, 42-48.

Drossman, D.A. (2006). The functional gastrointestinal disorders and the Rome III process. Gastroenterology *130*, 1377-1390.

Fahn, S., and Sulzer, D. (2004). Neurodegeneration and neuroprotection in Parkinson disease. NeuroRx *1*, 139-154.

Fasano, A., Visanji, N.P., Liu, L.W., Lang, A.E., and Pfeiffer, R.F. (2015). Gastrointestinal dysfunction in Parkinson's disease. Lancet Neurol *14*, 625-639.

Finn, T.P., Jones, R.E., Rich, C., Dahan, R., Link, J., David, C.S., Chou, Y.K., Offner, H., and Vandenbark, A.A. (2004). HLA-DRB1*1501 risk association in multiple sclerosis may not be related to presentation of myelin epitopes. J Neurosci Res *78*, 100-114.

Fujiwara, H., Hasegawa, M., Dohmae, N., Kawashima, A., Masliah, E., Goldberg, M.S., Shen, J., Takio, K., and Iwatsubo, T. (2002). alpha-Synuclein is phosphorylated in synucleinopathy lesions. Nat Cell Biol *4*, 160-164.

Fung, H.Y., Teryek, M., Lemenze, A.D., and Bergsbaken, T. (2022). CD103 fate mapping reveals that intestinal CD103(-) tissue-resident memory T cells are the primary responders to secondary infection. Sci Immunol *7*, eabl9925.

Garretti, F., Agalliu, D., Lindestam Arlehamn, C.S., Sette, A., and Sulzer, D. (2019). Autoimmunity in Parkinson's Disease: The Role of alpha-Synuclein-Specific T Cells. Front Immunol *10*, 303.

Gaublomme, J.T., Yosef, N., Lee, Y., Gertner, R.S., Yang, L.V., Wu, C., Pandolfi, P.P., Mak, T., Satija, R., Shalek, A.K., *et al.* (2015). Single-Cell Genomics Unveils Critical Regulators of Th17 Cell Pathogenicity. Cell *163*, 1400-1412.

Hamza, T.H., Zabetian, C.P., Tenesa, A., Laederach, A., Montimurro, J., Yearout, D., Kay, D.M., Doheny, K.F., Paschall, J., Pugh, E., *et al.* (2010). Common genetic variation in the HLA region is associated with late-onset sporadic Parkinson's disease. Nat Genet *42*, 781-785.

Hao, Y., Hao, S., Andersen-Nissen, E., Mauck, W.M., 3rd, Zheng, S., Butler, A., Lee, M.J., Wilk, A.J., Darby, C., Zager, M., *et al.* (2021). Integrated analysis of multimodal single-cell data. Cell *184*, 3573-3587 e3529.

Harms, A.S., Ferreira, S.A., and Romero-Ramos, M. (2021). Periphery and brain, innate and adaptive immunity in Parkinson's disease. Acta Neuropathol *141*, 527-545.

Harvey, D.C., Lacan, G., Tanious, S.P., and Melega, W.P. (2000). Recovery from methamphetamine induced long-term nigrostriatal dopaminergic deficits without substantia nigra cell loss. Brain Res *871*, 259-270.

Heinzel, S., Berg, D., Gasser, T., Chen, H., Yao, C., Postuma, R.B., and Disease, M.D.S.T.F.o.t.D.o.P.s. (2019). Update of the MDS research criteria for prodromal Parkinson's disease. Mov Disord *34*, 1464-1470.

Hill-Burns, E.M., Factor, S.A., Zabetian, C.P., Thomson, G., and Payami, H. (2011). Evidence for more than one Parkinson's disease-associated variant within the HLA region. PLoS One *6*, e27109.

Hirahara, K., Kokubo, K., Aoki, A., Kiuchi, M., and Nakayama, T. (2021). The Role of CD4(+) Resident Memory T Cells in Local Immunity in the Mucosal Tissue - Protection Versus Pathology. Front Immunol *12*, 616309.

Hotchkiss, A.J., and Gibb, J.W. (1980). Long-term effects of multiple doses of methamphetamine on tryptophan hydroxylase and tyrosine hydroxylase activity in rat brain. J Pharmacol Exp Ther *214*, 257-262.

Ivanov, II, McKenzie, B.S., Zhou, L., Tadokoro, C.E., Lepelley, A., Lafaille, J.J., Cua, D.J., and Littman, D.R. (2006). The orphan nuclear receptor RORgammat directs the differentiation program of proinflammatory IL-17+ T helper cells. Cell *126*, 1121-1133.

Kannarkat, G.T., Cook, D.A., Lee, J.K., Chang, J., Chung, J., Sandy, E., Paul, K.C., Ritz, B., Bronstein, J., Factor, S.A., *et al.* (2015). Common Genetic Variant Association with Altered HLA Expression, Synergy with Pyrethroid Exposure, and Risk for Parkinson's Disease: An Observational and Case-Control Study. NPJ Parkinsons Dis *1*.

Khare, M., Mangalam, A., Rodriguez, M., and David, C.S. (2005). HLA DR and DQ interaction in myelin oligodendrocyte glycoprotein-induced experimental autoimmune encephalomyelitis in HLA class II transgenic mice. J Neuroimmunol *169*, 1-12.

Khoo, T.K., Yarnall, A.J., Duncan, G.W., Coleman, S., O'Brien, J.T., Brooks, D.J., Barker, R.A., and Burn, D.J. (2013). The spectrum of nonmotor symptoms in early Parkinson disease. Neurology *80*, 276-281.

Ki, C.S., Stavrou, E.F., Davanos, N., Lee, W.Y., Chung, E.J., Kim, J.Y., and Athanassiadou, A. (2007). The Ala53Thr mutation in the alpha-synuclein gene in a Korean family with Parkinson disease. Clin Genet *71*, 471-473.

Kimball, E.S., Palmer, J.M., D'Andrea, M.R., Hornby, P.J., and Wade, P.R. (2005). Acute colitis induction by oil of mustard results in later development of an IBS-like accelerated upper GI transit in mice. Am J Physiol Gastrointest Liver Physiol *288*, G1266-1273.

Korsunsky, I., Millard, N., Fan, J., Slowikowski, K., Zhang, F., Wei, K., Baglaenko, Y., Brenner, M., Loh, P.R., and Raychaudhuri, S. (2019). Fast, sensitive and accurate integration of single-cell data with Harmony. Nat Methods *16*, 1289-1296.

Krogman, A., Tilahun, A., David, C.S., Chowdhary, V.R., Alexander, M.P., and Rajagopalan, G. (2017). HLA-DR polymorphisms influence in vivo responses to staphylococcal toxic shock syndrome toxin-1 in a transgenic mouse model. HLA *89*, 20-28.

Kruger, R., Kuhn, W., Muller, T., Woitalla, D., Graeber, M., Kosel, S., Przuntek, H., Epplen, J.T., Schols, L., and Riess, O. (1998). Ala30Pro mutation in the gene encoding alpha-synuclein in Parkinson's disease. Nat Genet *18*, 106-108.

Kulkarni, S., Micci, M.A., Leser, J., Shin, C., Tang, S.C., Fu, Y.Y., Liu, L., Li, Q., Saha, M., Li, C., *et al.* (2017). Adult enteric nervous system in health is maintained by a dynamic balance between neuronal apoptosis and neurogenesis. Proceedings of the National Academy of Sciences of the United States of America *114*, E3709-E3718.

Kurnik-Lucka, M., Pasieka, P., Laczak, P., Wojnarski, M., Jurczyk, M., and Gil, K. (2021). Gastrointestinal Dopamine in Inflammatory Bowel Diseases: A Systematic Review. Int J Mol Sci *22*.

Lange, J., Rivera-Ballesteros, O., and Buggert, M. (2022). Human mucosal tissue-resident memory T cells in health and disease. Mucosal Immunol *15*, 389-397.

Lebouvier, T., Neunlist, M., Bruley des Varannes, S., Coron, E., Drouard, A., N'Guyen, J.M., Chaumette, T., Tasselli, M., Paillusson, S., Flamand, M., *et al.* (2010). Colonic biopsies to assess the neuropathology of Parkinson's disease and its relationship with symptoms. PLoS One *5*, e12728.

Lengfeld, J.E., Lutz, S.E., Smith, J.R., Diaconu, C., Scott, C., Kofman, S.B., Choi, C., Walsh, C.M., Raine, C.S., Agalliu, I., *et al.* (2017). Endothelial Wnt/beta-catenin signaling reduces immune cell infiltration in multiple sclerosis. Proceedings of the National Academy of Sciences of the United States of America.

Lesage, S., Anheim, M., Letournel, F., Bousset, L., Honore, A., Rozas, N., Pieri, L., Madiona, K., Durr, A., Melki, R., *et al.* (2013). G51D alpha-synuclein mutation causes a novel parkinsonian-pyramidal syndrome. Ann Neurol *73*, 459-471.

Li, J., Olshansky, M., Carbone, F.R., and Ma, J.Z. (2016). Transcriptional Analysis of T Cells Resident in Human Skin. PLoS One *11*, e0148351.

Li, Z.S., Pham, T.D., Tamir, H., Chen, J.J., and Gershon, M.D. (2004). Enteric dopaminergic neurons: definition, developmental lineage, and effects of extrinsic denervation. J Neurosci *24*, 1330-1339.

Li, Z.S., Schmauss, C., Cuenca, A., Ratcliffe, E., and Gershon, M.D. (2006). Physiological modulation of intestinal motility by enteric dopaminergic neurons and the D2 receptor: analysis of dopamine receptor expression, location, development, and function in wild-type and knock-out mice. J Neurosci *26*, 2798-2807.

Lindestam Arlehamn, C.S., Dhanwani, R., Pham, J., Kuan, R., Frazier, A., Rezende Dutra, J., Phillips, E., Mallal, S., Roederer, M., Marder, K.S., *et al.* (2020). alpha-Synuclein-specific T cell reactivity is associated with preclinical and early Parkinson's disease. Nat Commun *11*, 1875.

Liu, B., Fang, F., Pedersen, N.L., Tillander, A., Ludvigsson, J.F., Ekbom, A., Svenningsson, P., Chen, H., and Wirdefeldt, K. (2017). Vagotomy and Parkinson disease: A Swedish register-based matched-cohort study. Neurology *88*, 1996-2002.

Liu, H., Koros, C., Strohaker, T., Schulte, C., Bozi, M., Varvaresos, S., Ibanez de Opakua, A., Simitsi, A.M., Bougea, A., Voumvourakis, K., *et al.* (2021). A Novel SNCA A30G Mutation Causes Familial Parkinson's Disease. Mov Disord *36*, 1624-1633.

Lutz, S.E., Smith, J.R., Kim, D.H., Olson, C.V., Ellefsen, K., Bates, J.M., Gandhi, S.P., and Agalliu, D. (2017). Caveolin1 is required for Th1 cell infiltration, but not tight junction remodeling, at the blood-brain barrier in autoimmune neuroinflammation. Cell reports *21*, 2104-2117.

Lyu, Y., Zhou, Y., and Shen, J. (2022). An Overview of Tissue-Resident Memory T Cells in the Intestine: From Physiological Functions to Pathological Mechanisms. Front Immunol *13*, 912393.

Main, B.S., Zhang, M., Brody, K.M., Ayton, S., Frugier, T., Steer, D., Finkelstein, D., Crack, P.J., and Taylor, J.M. (2016). Type-1 interferons contribute to the neuroinflammatory response and disease progression of the MPTP mouse model of Parkinson's disease. Glia *64*, 1590-1604.

Margolis, K.G., Li, Z., Stevanovic, K., Saurman, V., Israelyan, N., Anderson, G.M., Snyder, I., Veenstra-VanderWeele, J., Blakely, R.D., and Gershon, M.D. (2016). Serotonin transporter variant drives preventable gastrointestinal abnormalities in development and function. J Clin Invest *126*, 2221-2235.

Matheoud, D., Cannon, T., Voisin, A., Penttinen, A.M., Ramet, L., Fahmy, A.M., Ducrot, C., Laplante, A., Bourque, M.J., Zhu, L., *et al.* (2019). Intestinal infection triggers Parkinson's disease-like symptoms in Pink1(-/-) mice. Nature *571*, 565-569.

McLachlan, J.B., and Jenkins, M.K. (2007). Migration and accumulation of effector CD4+ T cells in nonlymphoid tissues. Proc Am Thorac Soc *4*, 439-442.

Metzger, J.M., and Emborg, M.E. (2019). Autonomic dysfunction in Parkinson disease and animal models. Clin Auton Res *29*, 397-414.

Miragaia, R.J., Gomes, T., Chomka, A., Jardine, L., Riedel, A., Hegazy, A.N., Whibley, N., Tucci, A., Chen, X., Lindeman, I., *et al.* (2019). Single-Cell Transcriptomics of Regulatory T Cells Reveals Trajectories of Tissue Adaptation. Immunity *50*, 493-504 e497.

Moschen, A.R., Adolph, T.E., Gerner, R.R., Wieser, V., and Tilg, H. (2017). Lipocalin-2: A Master Mediator of Intestinal and Metabolic Inflammation. Trends Endocrinol Metab *28*, 388-397.

Park, S., Kim, J., Chun, J., Han, K., Soh, H., Kang, E.A., Lee, H.J., Im, J.P., and Kim, J.S. (2019). Patients with Inflammatory Bowel Disease Are at an Increased Risk of Parkinson's Disease: A South Korean Nationwide Population-Based Study. J Clin Med *8*.

Pasanen, P., Myllykangas, L., Siitonen, M., Raunio, A., Kaakkola, S., Lyytinen, J., Tienari, P.J., Poyhonen, M., and Paetau, A. (2014). Novel alpha-synuclein mutation A53E associated with atypical

multiple system atrophy and Parkinson's disease-type pathology. Neurobiology of aging *35*, 2180 e2181-2185.

Peter, I., Dubinsky, M., Bressman, S., Park, A., Lu, C., Chen, N., and Wang, A. (2018). Anti-Tumor Necrosis Factor Therapy and Incidence of Parkinson Disease Among Patients With Inflammatory Bowel Disease. JAMA Neurol *75*, 939-946.

Pochard, C., Leclair-Visonneau, L., Coron, E., Neunlist, M., Rolli-Derkinderen, M., and Derkinderen, P. (2018). Cyclooxygenase 2 is upregulated in the gastrointestinal tract in Parkinson's disease. Mov Disord *33*, 493-494.

Polymeropoulos, M.H., Lavedan, C., Leroy, E., Ide, S.E., Dehejia, A., Dutra, A., Pike, B., Root, H., Rubenstein, J., Boyer, R., *et al.* (1997). Mutation in the alpha-synuclein gene identified in families with Parkinson's disease. Science *276*, 2045-2047.

Qin, X.Y., Zhang, S.P., Cao, C., Loh, Y.P., and Cheng, Y. (2016). Aberrations in Peripheral Inflammatory Cytokine Levels in Parkinson Disease: A Systematic Review and Meta-analysis. JAMA Neurol *73*, 1316-1324.

Rao, M., and Gershon, M.D. (2016). The bowel and beyond: the enteric nervous system in neurological disorders. Nat Rev Gastroenterol Hepatol *13*, 517-528.

Sampson, T.R., Debelius, J.W., Thron, T., Janssen, S., Shastri, G.G., Ilhan, Z.E., Challis, C., Schretter, C.E., Rocha, S., Gradinaru, V., *et al.* (2016). Gut Microbiota Regulate Motor Deficits and Neuroinflammation in a Model of Parkinson's Disease. Cell *167*, 1469-1480 e1412.

Shaw, L.A., Deng, T.Z., Omilusik, K.D., Takehara, K.K., Nguyen, Q.P., and Goldrath, A.W. (2022). Id3 expression identifies CD4(+) memory Th1 cells. Proceedings of the National Academy of Sciences of the United States of America *119*, e2204254119.

Sommer, A., Maxreiter, F., Krach, F., Fadler, T., Grosch, J., Maroni, M., Graef, D., Eberhardt, E., Riemenschneider, M.J., Yeo, G.W., *et al.* (2018). Th17 Lymphocytes Induce Neuronal Cell Death in a Human iPSC-Based Model of Parkinson's Disease. Cell stem cell *23*, 123-131 e126.

Soriano, M.A., Justicia, C., Ferrer, I., Rodriguez-Farre, E., and Planas, A.M. (1997). Striatal infarction in the rat causes a transient reduction of tyrosine hydroxylase immunoreactivity in the ipsilateral substantia nigra. Neurobiology of disease *4*, 376-385.

Stokholm, M.G., Danielsen, E.H., Hamilton-Dutoit, S.J., and Borghammer, P. (2016). Pathological alpha-synuclein in gastrointestinal tissues from prodromal Parkinson disease patients. Ann Neurol *79*, 940-949.

Sulzer, D., Alcalay, R.N., Garretti, F., Cote, L., Kanter, E., Agin-Liebes, J., Liong, C., McMurtrey, C., Hildebrand, W.H., Mao, X., *et al.* (2017). T cells from patients with Parkinson's disease recognize alpha-synuclein peptides. Nature *546*, 656-661.

Svensson, E., Horvath-Puho, E., Thomsen, R.W., Djurhuus, J.C., Pedersen, L., Borghammer, P., and Sorensen, H.T. (2015). Vagotomy and subsequent risk of Parkinson's disease. Ann Neurol *78*, 522-529.

Swarnalekha, N., Schreiner, D., Litzler, L.C., Iftikhar, S., Kirchmeier, D., Kunzli, M., Son, Y.M., Sun, J., Moreira, E.A., and King, C.G. (2021). T resident helper cells promote humoral responses in the lung. Sci Immunol *6*.

Tanemoto, S., Sujino, T., Miyamoto, K., Moody, J., Yoshimatsu, Y., Ando, Y., Koya, I., Harada, Y., Tojo, A.O., Ono, K., *et al.* (2022). Single-cell transcriptomics of human gut T cells identifies cytotoxic CD4(+)CD8A(+) T cells related to mouse CD4 cytotoxic T cells. Front Immunol *13*, 977117.

Tysnes, O.B., Kenborg, L., Herlofson, K., Steding-Jessen, M., Horn, A., Olsen, J.H., and Reichmann, H. (2015). Does vagotomy reduce the risk of Parkinson's disease? Ann Neurol *78*, 1011-1012.

von Hoesslin, M., Kuhlmann, M., de Almeida, G.P., Kanev, K., Wurmser, C., Gerullis, A.K., Roelli, P., Berner, J., and Zehn, D. (2022). Secondary infections rejuvenate the intestinal CD103(+) tissue-resident memory T cell pool. Sci Immunol *7*, eabp9553.

Wang, Y.C., Cao, Y., Pan, C., Zhou, Z., Yang, L., and Lusis, A.J. (2023). Intestinal cell type-specific communication networks underlie homeostasis and response to Western diet. J Exp Med *220*.

Williams, G.P., Schonhoff, A.M., Jurkuvenaite, A., Gallups, N.J., Standaert, D.G., and Harms, A.S. (2021). CD4 T cells mediate brain inflammation and neurodegeneration in a mouse model of Parkinson's disease. Brain *144*, 2047-2059.

Wolinsky, E., and Patterson, P.H. (1983). Tyrosine hydroxylase activity decreases with induction of cholinergic properties in cultured sympathetic neurons. J Neurosci *3*, 1495-1500.

Yang, J., Sundrud, M.S., Skepner, J., and Yamagata, T. (2014). Targeting Th17 cells in autoimmune diseases. Trends Pharmacol Sci *35*, 493-500.

Yenyuwadee, S., Sanchez-Trincado Lopez, J.L., Shah, R., Rosato, P.C., and Boussiotis, V.A. (2022). The evolving role of tissue-resident memory T cells in infections and cancer. Sci Adv *8*, eabo5871.

Yokoi, T., Murakami, M., Kihara, T., Seno, S., Arase, M., Wing, J.B., Sondergaard, J.N., Kuwahara, R., Minagawa, T., Oguro-Igashira, E., *et al.* (2023). Identification of a unique subset of tissue-resident memory CD4(+) T cells in Crohn's disease. Proceedings of the National Academy of Sciences of the United States of America *120*, e2204269120.

Yoo, B.B., and Mazmanian, S.K. (2017). The Enteric Network: Interactions between the Immune and Nervous Systems of the Gut. Immunity *46*, 910-926.

Yoshino, H., Hirano, M., Stoessl, A.J., Imamichi, Y., Ikeda, A., Li, Y., Funayama, M., Yamada, I., Nakamura, Y., Sossi, V., *et al.* (2017). Homozygous alpha-synuclein p.A53V in familial Parkinson's disease. Neurobiology of aging *57*, 248 e247-248 e212.

Zarranz, J.J., Alegre, J., Gomez-Esteban, J.C., Lezcano, E., Ros, R., Ampuero, I., Vidal, L., Hoenicka, J., Rodriguez, O., Atares, B., *et al.* (2004). The new mutation, E46K, of alpha-synuclein causes Parkinson and Lewy body dementia. Ann Neurol *55*, 164-173.

Zundler, S., Becker, E., Spocinska, M., Slawik, M., Parga-Vidal, L., Stark, R., Wiendl, M., Atreya, R., Rath, T., Leppkes, M., *et al*. (2019). Hobit- and Blimp-1-driven CD4(+) tissue-resident memory T cells control chronic intestinal inflammation. Nat Immunol *20*, 288-300.

FIGURE LEGENDS

Figure 1. α-Syn$_{32-46}$ immunizations induce weight loss in HLA DRB1*15:01, but not wild-type, mice. **(A)** A schematic diagram of the experimental design. Wild-type (WT) and HLA mice were immunized with PBS, CFA only, or CFA/ α-syn$_{32-46}$ peptide and received a boost after two weeks. At 14 and 16 DPI, an intravenous injection of *B. pertussis* toxin (Ptx) was administered. Mice were monitored daily for signs of illness and change in weight. **(B)** Pie charts show the fraction of WT (top) - and HLA (bottom) - immunized mice that were healthy (light purple), became ill (dark purple) or died (gray). (**C, D**) Graphs of percentage weight change from the initial weight (0 DPI) for WT **(C)**, and HLA **(D)** mice immunized with either PBS (grey triangles), CFA only (black circles), or CFA/α-syn$_{32-46}$ peptide (green triangles). The red dashed lines indicate the time when mice received an immunization boost and PTx injections at 14 and 16 DPI, respectively. **(E)** Graph depicting the percentage of weight loss for CFA only and sick CFA/α-syn$_{32-46}$ HLA mice. The data in (**E**) were analyzed using a mixed-effect ANOVA for repeated measurements followed by Bonferroni post-hoc correction; * $p<0.05$. **WT**: CFA only (n= 23 mice), CFA/ α-syn$_{32-46}$ peptide (n=25 mice). **HLA**: PBS (n=16 mice), CFA only (n=34 mice), CFA/ α-syn$_{32-46}$ peptide (n=35 mice).

Figure 2. Total GI transit time is delayed in CFA/α-syn$_{32-46}$ -immunized HLA mice. (A, B) Schematic diagrams of the experimental design for immunization and gastrointestinal (GI) transit time. Mice were gavaged with a non-absorbable carmine red mixture. The time from the oral gavage to the release of a red fecal pellet was recorded as the total gastrointestinal (GI) transit time. The total GI time was measured at 21, 25, and 35 days post-immunization (DPI). (**C, D**) Dotted bar graphs depicting the total GI transit time at 21 DPI for either all **(C)**, or sick **(D)**, PBS (empty circles), CFA only (black) and CFA/α-syn$_{32-46}$ (green)- immunized HLA mice. (**E, F**) Dotted bar graphs depicting the total GI transit time of CFA only (black) and CFA/α-syn$_{32-46}$ (green)-immunized HLA mice at 25 **(E)** and 35 **(F)** DPI. (**G, H**) Correlation

graphs between peak weight loss and total GI transit time of CFA only **(G)**, and CFA/α-syn$_{32-46}$ **(H)** - immunized HLA mice. Dark purple circles represent sick and light purple circles represent healthy mice. **(I)** Bar graphs of the total GI transit time of WT (dark bars) and HLA (light bars) immunized with CFA only (black circles) or CFA/α-syn$_{32-46}$ (green circles). Only sick CFA/α-syn$_{32-46}$-immunized HLA mice are shown. Data were analyzed by Mann-Whitney test (**C, D**), Pearson correlation (**G, H**) and two-way ANOVA (**I**); ** $p<0.01$, *** $p<0.001$, **** $p<0.0001$. Dotted bar graphs represent the mean and SEM. Each symbol represents data from one animal. **WT**: CFA only n=13 mice, CFA/α-syn$_{32-46}$ n=14 mice. **HLA**: PBS n=7 mice, CFA only n=20 mice, CFA/α-syn$_{32-46}$ n=21 mice. WT: 2 independent experiments, HLA: 5 independent experiments.

Figure 3. α-Syn$_{32-46}$ immunizations induce enteric neuron loss in HLA DRB1*15:01 mice. (A, B) Schematic diagram of the experimental design and the myenteric and submucosal plexuses of the ileum used for the flat mount analysis. (**C-H**) Representative images of the myenteric **(C-E),** and submucosal (**F-H**) plexuses stained for DAPI (blue), TH (green), and ANNA1 (red). Thin white arrows indicate cell bodies of dopaminergic neurons; white arrowheads indicate dopaminergic neuronal processes. Scale bars = 75 μm. (**I-N**) Dotted bar graphs of ANNA1$^+$ **(I)** and TH$^+$ **(J)** neurons per mm^2 in the myenteric plexus, ANNA1$^+$ **(K),** or TH$^+$ **(L)** neurons per mm^2, area covered **(M)** and mean fluorescence intensity (MFI) **(N)** of the TH signal in the submucosal plexus of PBS (empty circles), CFA only (black circles) and CFA/α-syn$_{32-46}$ (green circles)-immunized HLA mice. Dotted bar graphs show the mean and error bars the SEM. Data were analyzed by one-way ANOVA test. * $p<0.05$, ** $p<0.01$. PBS, n= 14; CFA only n=15 mice; CFA/α-syn$_{32-46}$ n=20 (myenteric) and 18 (submucosal) HLA mice; data collected from 6 independent experiments.

Figure 4. Neuronal loss begins after 18 days post-immunization in CFA/α-syn$_{32-46}$ -immunized HLA DRB1*15:01 mice. (A, B) Schematic diagram of the experimental design (**A**) and the myenteric and submucosal plexuses of the ileum (**B**) used for analysis. HLA DRB1*15:01 mice were immunized with CFA only or CFA/α-syn$_{32-46}$ and received a boost after two weeks. At 14 and 16 DPI, *B. pertussis* toxin (Ptx) was administered intravenously. At 18 and 42 DPI, the ileum was dissected out for analysis. **(C-F)** Representative images of the myenteric and submucosal plexuses at 18 DPI stained for DAPI (blue), TH (green), and ANNA1 (red). (**G, H**) Dotted bar graphs depicting the number of ANNA1$^+$ **(G)** and TH$^+$ **(H)** neurons in the myenteric plexuses of CFA only (black circles) and CFA/α-syn$_{32-46}$ (green circles)-immunized mice at 18 DPI. (**I, J**) Dotted bar graphs of ANNA1$^+$ **(I)** and TH$^+$ cells **(J)** in the submucosal plexuses of CFA only (black circles) and CFA/α-syn$_{32-46}$ (green circles)-immunized mice at 18 DPI. (**K, L**) Dotted bar graphs of the TH area **(K)** and mean fluorescence intensity (MFI) **(L)** of TH signal in the submucosal plexus of CFA only (black circles) and CFA/α-syn$_{32-46}$ (green circles)-immunized mice at 18 DPI. **(M-P)** Representative images of the myenteric and submucosal plexuses at 42 DPI stained for DAPI (blue), TH (green), and ANNA1 (red). (**Q, R**) Dotted bar graphs of ANNA1$^+$ **(Q)** and TH$^+$ cells **(R)** in the myenteric plexus of CFA only (black circles) and CFA/α-syn$_{32-46}$ (green circles)-immunized mice at 42 DPI. (**S-V**) Dotted bar graphs of ANNA1$^+$ **(S)**, and TH$^+$ cells **(T), TH** area **(U)** and mean fluorescence intensity (MFI) **(V)** of TH signal in the submucosal plexus of CFA only (black circles) and CFA/α-syn$_{32-46}$ (green circles)-immunized mice at 42 DPI. Dotted bar graphs show the mean and error bars the SEM. Each symbol represents data collected from a mouse. Data were analyzed by a two-tailed Student t-test. * $p<0.05$, ** $p<0.01$. 18 DPI: CFA only n=5 mice, CFA/α-syn$_{32-46}$ n=5 mice; 42 DPI: CFA only n=6-7 mice, CFA/α-syn$_{32-46}$ n=6 mice (data were collected from one experiment). (**C-F; M-P**) Scale bars = 50 μm.

Figure 5. Gene signatures associated with the innate and adaptive immune responses and altered T_H1/T_H17 gene signatures are present in the small intestine of α-syn$_{32-46}$-immunized HLA mice. (A) Schematic diagram of the experimental design for bulk and single-cell RNA seq (bulk RNA sequencing: CFA only n=4 mice, CFA/α-syn$_{32-46}$ n=4 mice; single cell RNA sequencing: PBS n=2 mice, CFA n=3 mice, CFA/α-syn$_{32-46}$ n=3 mice). **(B)** A volcano plot of differentially expressed genes from bulk RNA seq of the ileums of CFA/α-syn$_{32-46}$ versus CFA only- immunized HLA mice at 21 DPI. Significantly down-regulated (blue) and up-regulated (red) genes are plotted by fold change on the x-axis and the adjusted p-value on the y-axis. Red lines indicate adjusted p values (p_{adj}) ≤ 0.05 and $|\log_2$ fold change$| \geq 0.5$ which were used to identify statistically significant, differentially expressed genes. Genes of interest are highlighted in green and labeled. **(C)** GO enrichment bar graph depicting five functional categories of upregulated genes from the ileum of α-syn$_{32-46}$ immunized HLA mice at 21 DPI. Red diamonds indicate the number of genes represented by the GO term, and gray bars indicate -$\log_2$(FDR) values. GO terms are considered significant with a false discovery rate (FDR) < 0.05. **(D)** UMAP representation of single cell RNA sequencing (scRNAseq) data of $CD45^+$ cells sorted from the small intestine of all three conditions (PBS, CFA, CFA/α-syn$_{32-46}$). **(E)** Bar graph showing the proportion of sequenced $CD45^+$ cells for each cluster of the UMAP (1-27 cell populations). Each bar shows the relative proportions of $CD45^+$ cells for each condition [PBS (purple), CFA only (teal), CFA/α-syn$_{32-46}$ (orange)] corrected for the number of cells sequenced from each condition. The underlined clusters are overrepresented (>45% of cluster) by cells isolated from CFA/α-syn$_{32-46}$ HLA mice. **(F)** UMAP projections of T_H1 and T_H17 clusters isolated from the dataset [PBS (purple), CFA only (teal), CFA/α-syn$_{32-46}$ (orange)]. **(G)** Heatmap of the average expression of 20 tissue-resident-memory (T_{RM})-associated genes in Th1 and Th17 cells, separated by condition. Bolded gene names are significantly upregulated in the Th1 population (p_{adj} < 0.05) from CFA/α-syn$_{32-46}$ - compared to CFA only-immunized HLA mice. Underlined gene names are significantly upregulated in the T_H17 population (p_{adj} < 0.05) in CFA/α-syn$_{32-46}$ compared to CFA only-immunized

HLA mice. **(H)** UMAP projection of the T_H1 cell subset with a bar graph of the proportion of T_H1 subclusters as a percent of total T_H1 cells by condition. Each bar shows the relative proportions of cells from each condition [PBS (purple), CFA only (teal), CFA/α-syn$_{32-46}$ (orange)] corrected for the number of total T_H1 cells from each treatment. **(I)** Feature plots of T_{RM} genes from panel **G**, *Tnfrsf4*, and *Fosl2* in the T_H1 cluster. **(J)** Violin plots of *Bcl2*, *Il7r*, *Tnfrsf4*, *Ramp3*, *Crem*, *Ifngr1*, *Vps37b*, and *Fosl2* gene expression in the T_H1 cluster, separated by condition. Statistical analyses were done by Wilcoxon Rank Sum test, followed by Bonferroni correction for multiple comparisons. **(K)** UMAP projection of the T_H17 cell subset with a bar graph of the proportion of T_H17 subcluster as a percent of total T_H17 cells by condition. Each bar shows the relative proportions of cells from condition [PBS (purple), CFA only (teal), CFA/α-syn$_{32-46}$ (orange)] corrected for the number of cells from each treatment within the T_H17 cluster. **(L)** Feature plots of T_{RM} genes (**from Fig. 5G**), *Ifng*, and *Il17a* in the T_H17 cluster. **(M)** Violin plots of *Bcl2*, *Il7r*, *Ramp3*, *Rgs2*, *Samsn1*, *Crem*, *Cd69*, *Ifng*, and *Il22* gene expression in the T_H17 cluster, separated by immunization treatment. For statistical significance: * $p_{adj} < 0.05$, ** $p_{adj} < 0.01$, *** $p_{adj} < 0.001$, **** $p_{adj} < 0.0001$.

Figure 6. CD4$^+$ T cell depletion partially rescues neuronal loss in α-syn$_{32-46}$ immunized HLA mice. **(A)** A schematic diagram of the experimental design. HLA mice were immunized with CFA/α-syn$_{32-46}$ peptide and received a boost after two weeks. At 14 and 16 DPI, *B. pertussis* toxin (Ptx) was administered intravenously. Mice received α-CD4 or isotype control antibodies intraperitoneally at -3 and -1 DPI (white arrows) and then at weekly intervals. Mice received α-CD8 antibodies intraperitoneally at -2 DPI (black arrows) and then at 10-day intervals. At 28 DPI, the ileum was dissected out for analysis. **(B)** Graph showing the levels of CD4$^+$ or CD8$^+$ T cells as % of CD45$^+$ cells at three distinct DPIs in CFA/α-syn$_{32-46}$ HLA mice for each treatment: α-CD4 (red), α-CD8 (teal), or isotype control (gray). **(C)** Kaplan Meier curve depicting the probability of survival and **(D)** pie charts displaying the proportion of α-CD4

(red)-, α-CD8 (teal)-, or isotype control (gray)-treated CFA/α-syn$_{32-46}$ HLA mice that remained healthy (light purple), became ill (dark purple) or died (gray). **(E)** Graph depicting the percent of weight change from the initial weight (0 DPI) of α-CD4 (red)-, α-CD8 (teal)-, or isotype control (gray)-treated CFA/α-syn$_{32-46}$-immunized HLA mice. **(F)** Dotted bar graph depicting the total GI transit time of α-CD4 (red)-, α-CD8 (teal)-, or isotype control (gray)-treated CFA/α-syn$_{32-46}$ HLA mice. **(G-I)** Representative fluorescent images of the submucosal plexus of Isotype control **(G)**, α-CD4 **(H)**, α-CD8 **(I)** treated CFA/α-syn$_{32-46}$ HLA mice stained with DAPI (blue), TH (green) and ANNA1 (red). White arrowheads indicate TH$^+$ cell bodies. Scale bar = 100 µm. **(J-Q)** Dotted bar graphs depicting the number of dopaminergic neurons **(J, K)**, TH$^+$ MFI **(L)**, TH$^+$ area **(M)**, all neurons **(N, O)**, and macrophages **(P, Q)** in the myenteric and submucosal plexuses of α-CD4 (red)-, α-CD8 (teal)-, or isotype control (gray)-treated CFA/α-syn$_{32-46}$ HLA mice. Data analyzed by repeated-measure ANOVA (**B, C**), and two-way ANOVA (**G-N**). Bar graphs depict the mean and error bars the SEM. Each symbol in the bar graphs represents the data collected from one mouse. *$p<0.05$, ***$p<0.001$, **** $p<0.0001$. Isotype control n = 8 mice, α-CD4 n = 10 mice, α-CD8 n = 8, data collected from 3 independent experiments.

Figure 7. The role of α-syn-specific T cells in PD pathogenesis. α-Syn-specific T cells have been identified in PD patients carriers of the HLA DRB1*15:01 allele. Humanized mice, lacking MHCII$^{-/-}$ and expressing HLA DRB1*15:01, that are immunized with the α-syn$_{32-46}$ peptide may produce α-syn-specific T cells (T_H1 and T_H17 lymphocytes; blue) in the peripheral lymphoid organs (spleen and lymph nodes). These T cells (blue) leave the circulation to home to target organs, where they may acquire a putative "resident memory" phenotype (yellow). We postulate that the gut is one such organ where T_H1/ T_H17 cells (blue) are converted to mucosal T_{RM} (yellow) found normally during infection or chronic inflammation based on our single cell RNA sequencing data. In addition, signatures of both innate and adaptive immune responses are upregulated in the gut with CFA/α-syn$_{32-46}$ peptide immunizations based

on bulk RNA sequencing. The activation of both innate and adaptive immune responses in CFA/α-syn$_{32-46}$-immunized HLA mice may trigger enteric neurodegeneration in the submucosal plexus. However, there is neither inflammation nor T cell infiltration into the brains of α-syn$_{32-46}$-immunized HLA mice, suggesting that additional factors are required to induce the CNS neuropathology and behavioral phenotypes characteristic of PD.

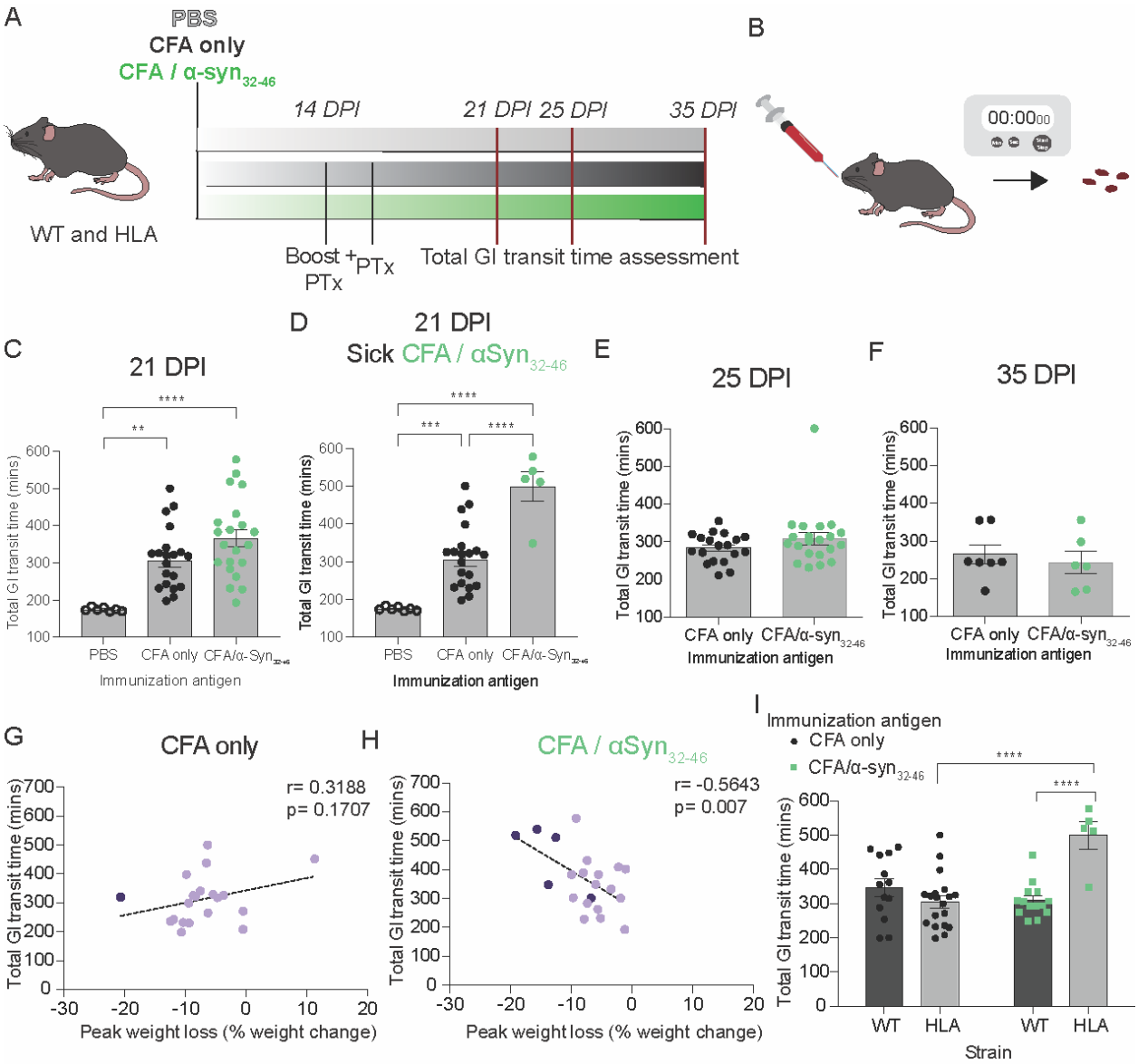
A
PBS
CFA only
CFA / α-syn32-46
14 DPI
21 DPI
25 DPI
35 DPI
WT and HLA
Boost + PTx
PTx
Total GI transit time assessment
B
00:00
C
21 DPI
Total GI transit time (mins)
PBS
CFA only
CFA/α-Syn32-46
Immunization antigen
D
21 DPI
Sick CFA / αSyn32-46
E
25 DPI
F
35 DPI
CFA only
CFA/α-syn32-46
Immunization antigen
G
CFA only
r= 0.3188
p= 0.1707
Peak weight loss (% weight change)
H
CFA / αSyn32-46
r= -0.5643
p= 0.007
I
Immunization antigen
CFA only
CFA/α-syn32-46
WT
HLA
Strain

Figure 1

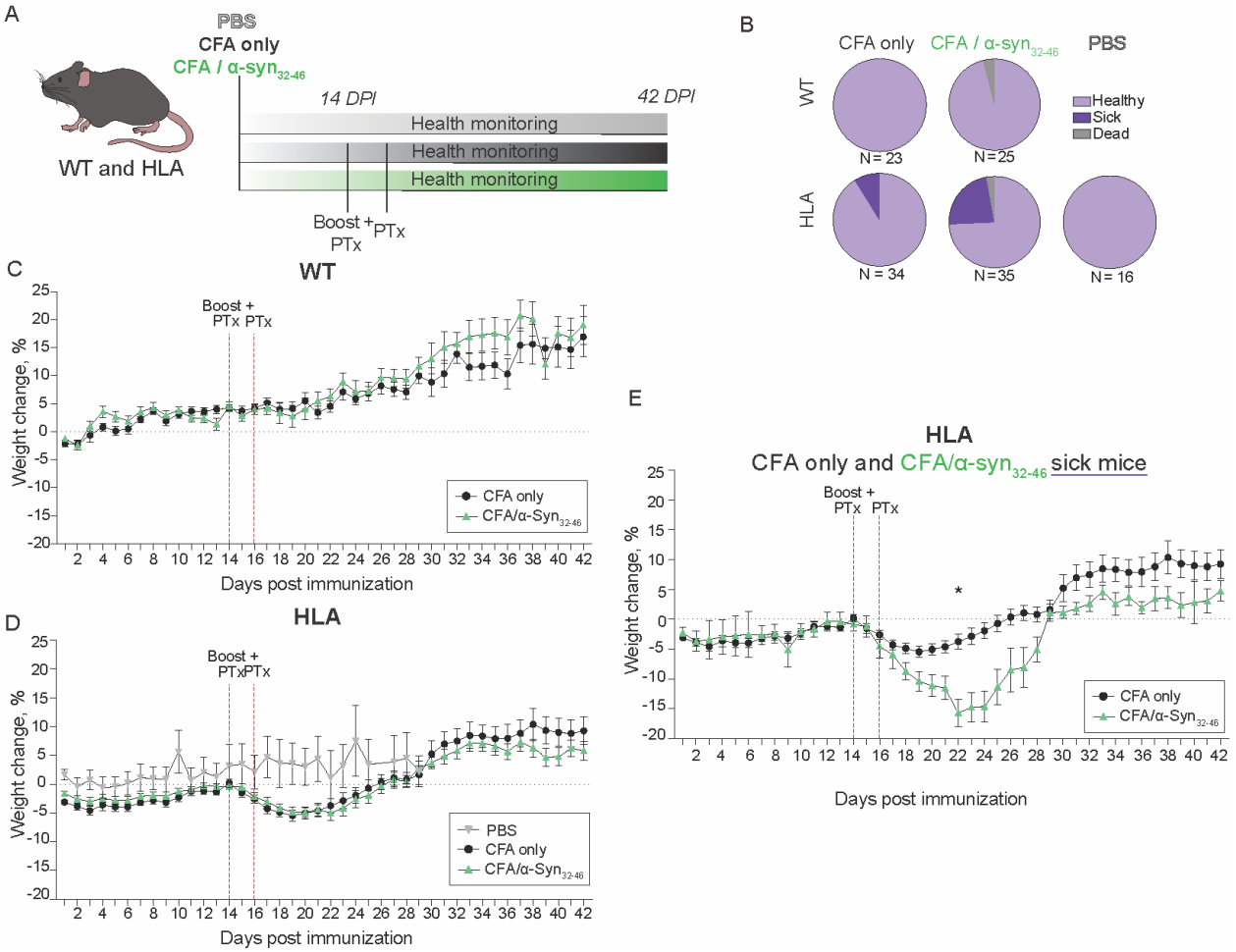
A
PBS
CFA only
CFA / α-syn32-46
WT and HLA
14 DPI
42 DPI
Health monitoring
Health monitoring
Health monitoring
Boost + PTx
PTx
B
CFA only
CFA / α-syn32-46
PBS
WT
HLA
Healthy
Sick
Dead
N = 23
N = 25
N = 34
N = 35
N = 16
C
WT
Boost + PTx PTx
Weight change, %
Days post immunization
CFA only
CFA/α-Syn32-46
D
HLA
Boost + PTxPTx
Weight change, %
Days post immunization
PBS
CFA only
CFA/α-Syn32-46
E
HLA
CFA only and CFA/α-syn32-46 sick mice
Boost + PTx PTx
Weight change, %
Days post immunization
CFA only
CFA/α-Syn32-46

Figure 2

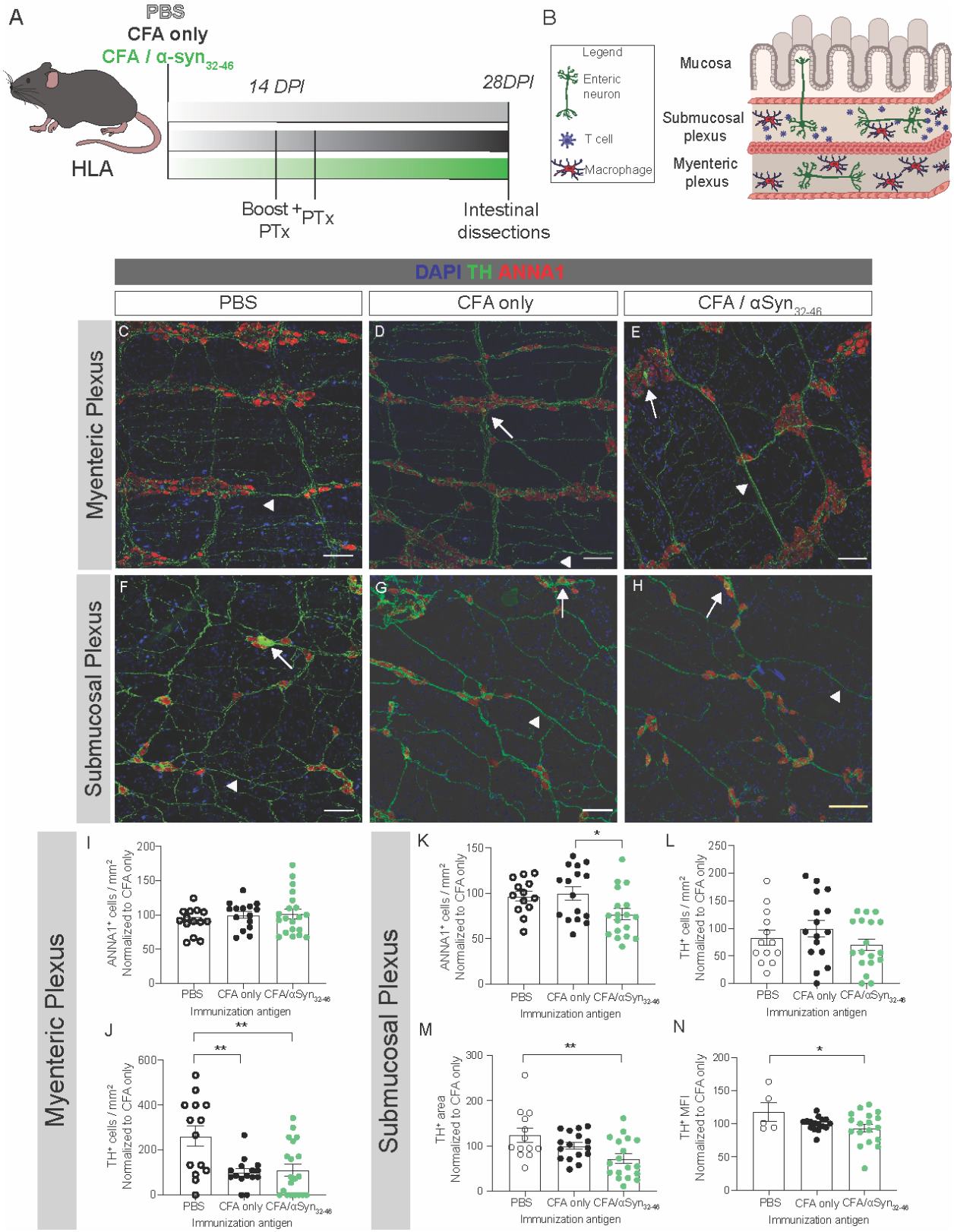
A
PBS
CFA only
CFA / α-syn32-46
HLA
14 DPI
28DPI
Boost + PTx
PTx
Intestinal dissections
B
Legend
Enteric neuron
T cell
Macrophage
Mucosa
Submucosal plexus
Myenteric plexus
DAPI TH ANNA1
PBS
CFA only
CFA / αSyn32-46
Myenteric Plexus
Submucosal Plexus
C
D
E
F
G
H
I
J
K
L
M
N
ANNA1+ cells / mm2 Normalized to CFA only
TH+ cells / mm2 Normalized to CFA only
TH+ area Normalized to CFA only
TH+ MFI Normalized to CFA only
PBS
CFA only
CFA/αSyn32-46
Immunization antigen

Figure 3

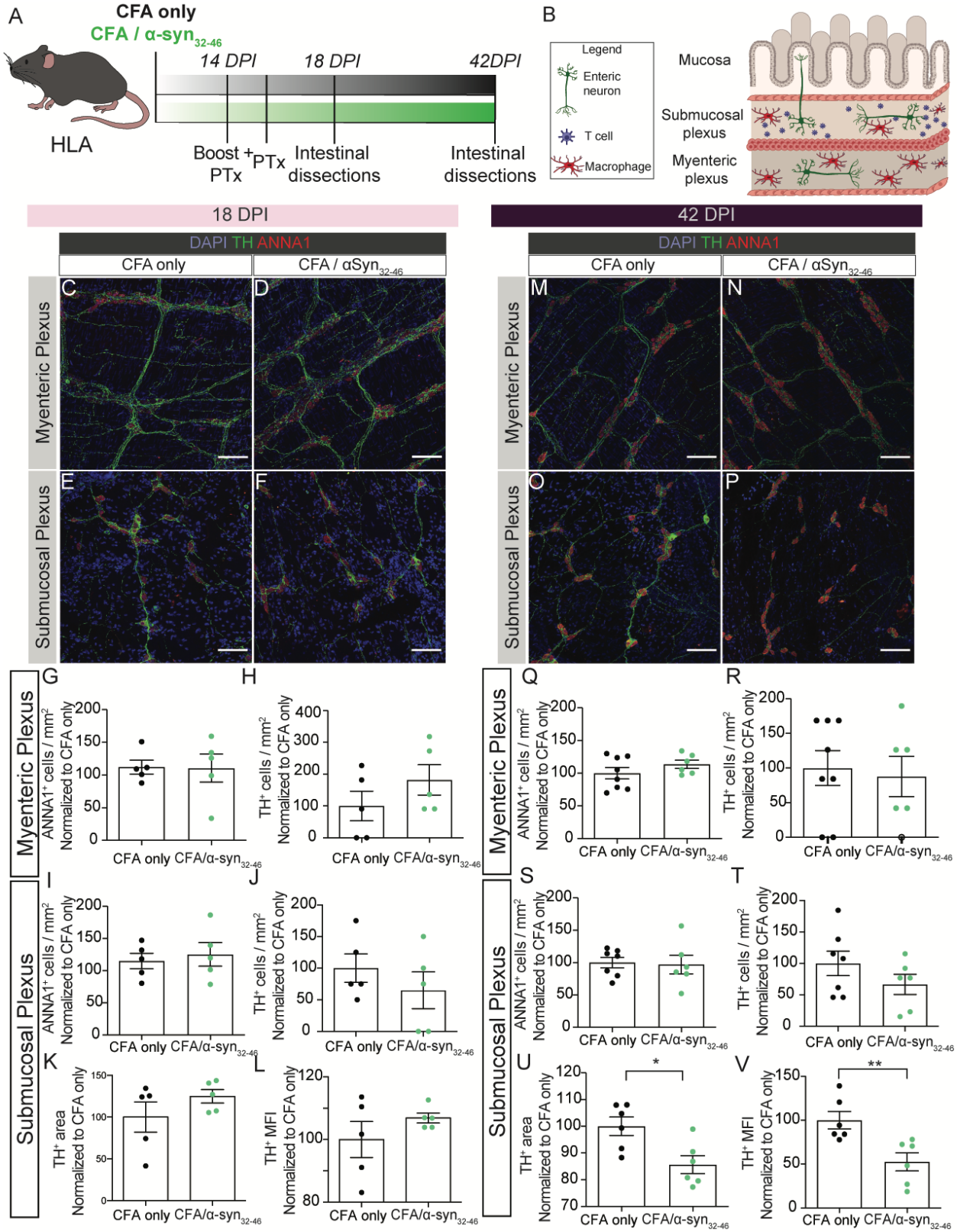
A
CFA only
CFA / α-syn32-46
HLA
14 DPI
18 DPI
42DPI
Boost + PTx
PTx
Intestinal dissections
Intestinal dissections
B
Legend
Enteric neuron
T cell
Macrophage
Mucosa
Submucosal plexus
Myenteric plexus
18 DPI
42 DPI
DAPI TH ANNA1
CFA only
CFA / αSyn32-46
Myenteric Plexus
Submucosal Plexus
C
D
E
F
M
N
O
P
G
H
I
J
K
L
Q
R
S
T
U
V
ANNA1+ cells / mm2 Normalized to CFA only
TH+ cells / mm2 Normalized to CFA only
TH+ area Normalized to CFA only
TH+ MFI Normalized to CFA only
CFA only
CFA/α-syn32-46
*
**

Figure 4

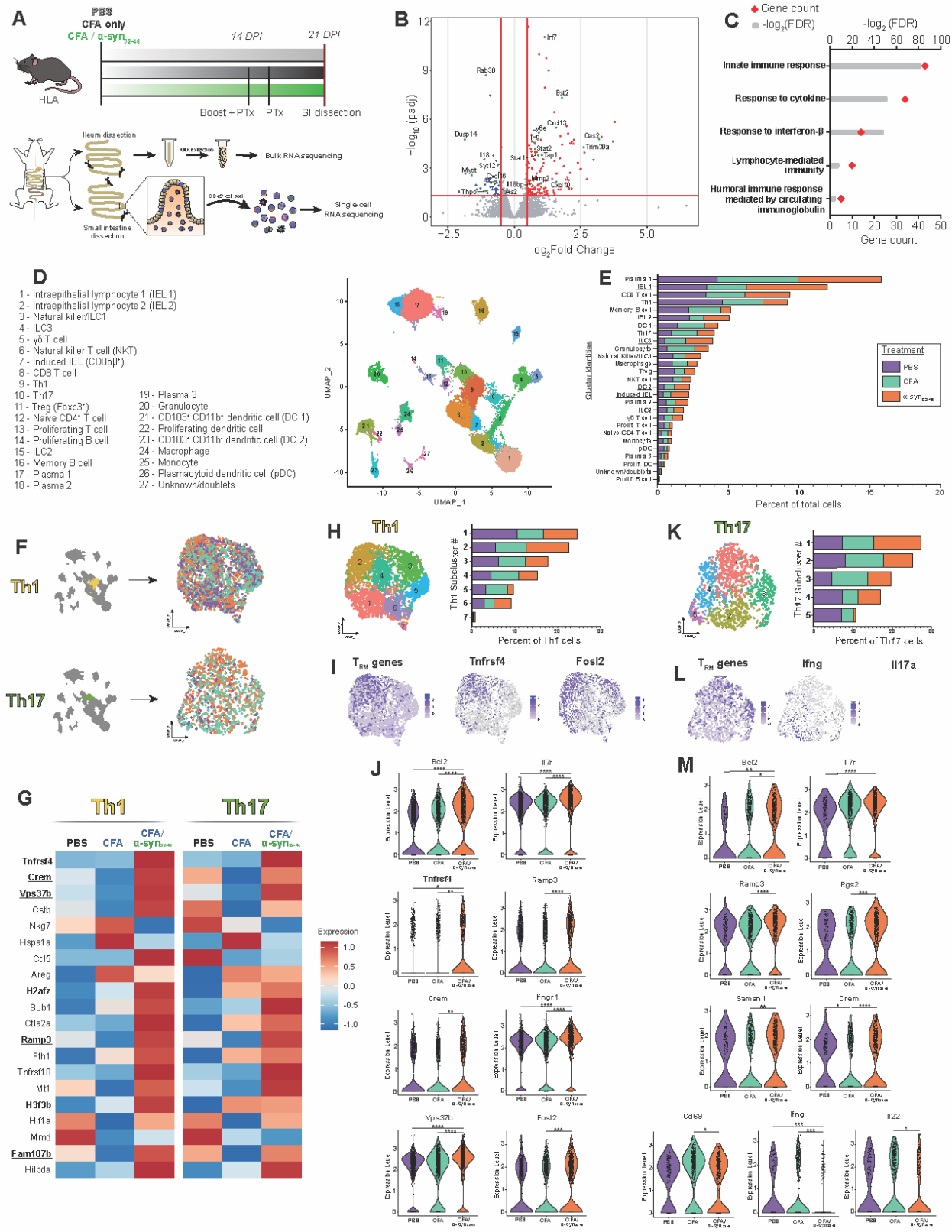
A
PBS
CFA only
CFA / α-syn
14 DPI
21 DPI
HLA
Boost + PTx
PTx
SI dissection
Ileum dissection
Bulk RNA sequencing
Small intestine dissection
Single-cell RNA sequencing
B
−log10 (padj)
log2Fold Change
C
Gene count
-log2(FDR)
Innate immune response
Response to cytokine
Response to interferon-β
Lymphocyte-mediated immunity
Humoral immune response mediated by circulating immunoglobulin
Gene count
D
1 - Intraepithelial lymphocyte 1 (IEL 1)
2 - Intraepithelial lymphocyte 2 (IEL 2)
3 - Natural killer/ILC1
4 - ILC3
5 - γδ T cell
6 - Natural killer T cell (NKT)
7 - Induced IEL (CD8αβ+)
8 - CD8 T cell
9 - Th1
10 - Th17
11 - Treg (Foxp3+)
12 - Naive CD4+ T cell
13 - Proliferating T cell
14 - Proliferating B cell
15 - ILC2
16 - Memory B cell
17 - Plasma 1
18 - Plasma 2
19 - Plasma 3
20 - Granulocyte
21 - CD103+ CD11b+ dendritic cell (DC 1)
22 - Proliferating dendritic cell
23 - CD103+ CD11b- dendritic cell (DC 2)
24 - Macrophage
25 - Monocyte
26 - Plasmacytoid dendritic cell (pDC)
27 - Unknown/doublets
UMAP_1
UMAP_2
E
Treatment
PBS
CFA
Percent of total cells
F
Th1
Th17
H
Th1
Th1 Subcluster #
Percent of Th1 cells
K
Th17
Th17 Subcluster #
Percent of Th17 cells
I
TRM genes
Tnfrsf4
Fosl2
L
TRM genes
Ifng
Il17a
G
Th1
Th17
PBS
CFA
CFA/ α-syn
Tnfrsf4
Crem
Vps37b
Cstb
Nkg7
Hspa1a
Ccl5
Areg
H2afz
Sub1
Ctla2a
Ramp3
Fth1
Tnfrsf18
Mt1
H3f3b
Hif1a
Mmd
Fam107b
Hilpda
Expression
J
Bcl2
Il7r
Tnfrsf4
Ramp3
Crem
Ifngr1
Vps37b
Fosl2
M
Bcl2
Il7r
Ramp3
Rgs2
Samsn1
Crem
Cd69
Ifng
Il22
Expression Level

Figure 5

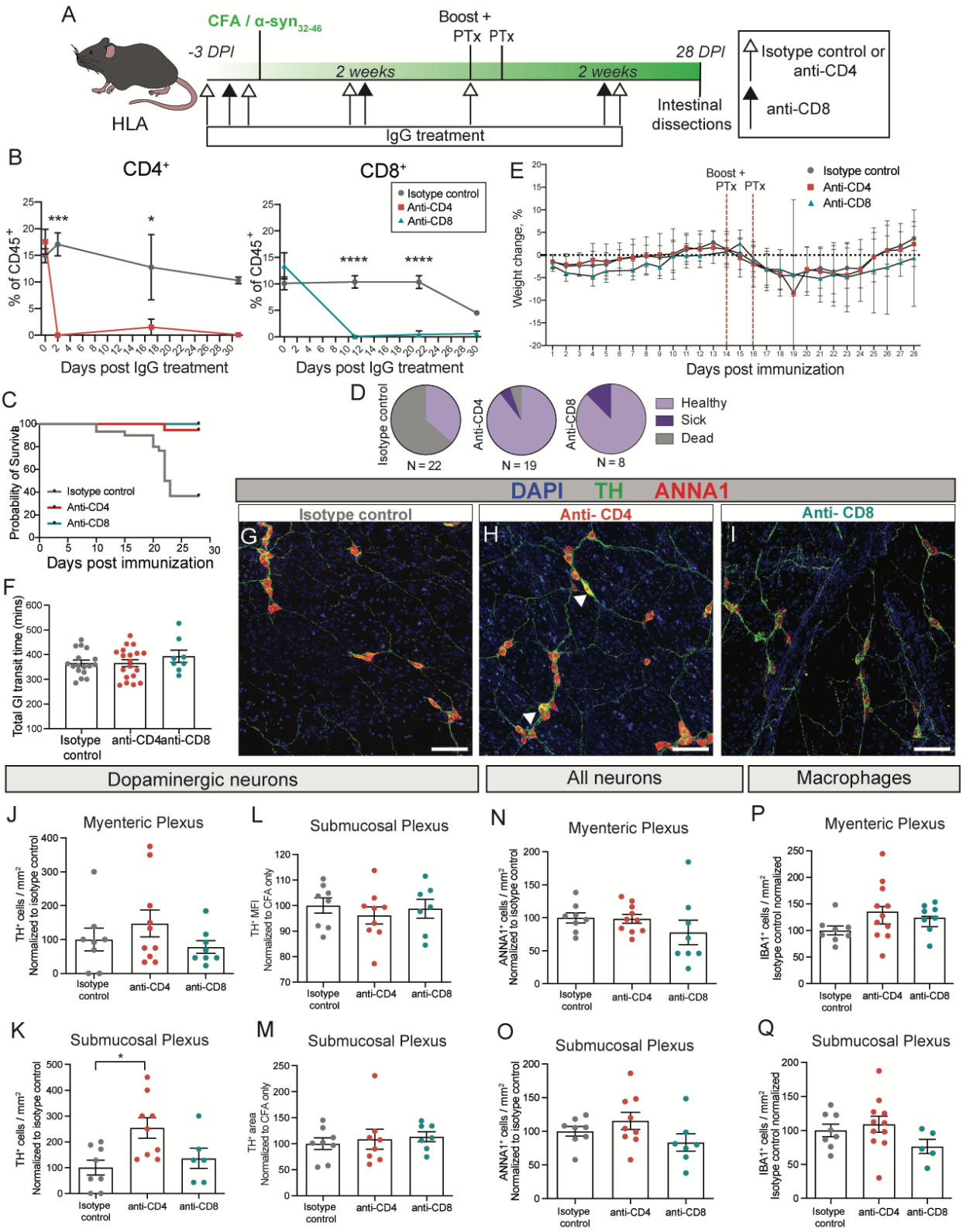
A
CFA / α-syn32-46
-3 DPI
Boost +
PTx PTx
28 DPI
2 weeks
2 weeks
HLA
IgG treatment
Intestinal dissections
Isotype control or anti-CD4
anti-CD8
B
CD4+
CD8+
% of CD45+
Days post IgG treatment
Isotype control
Anti-CD4
Anti-CD8
E
Weight change, %
Days post immunization
C
Probability of Survival
Days post immunization
D
Isotype control
Anti-CD4
Anti-CD8
N = 22
N = 19
N = 8
Healthy
Sick
Dead
F
Total GI transit time (mins)
Isotype control
anti-CD4
anti-CD8
DAPI TH ANNA1
Isotype control
Anti- CD4
Anti- CD8
G
H
I
Dopaminergic neurons
All neurons
Macrophages
J
Myenteric Plexus
TH+ cells / mm2 Normalized to isotype control
L
Submucosal Plexus
TH+ MFI Normalized to CFA only
N
Myenteric Plexus
ANNA1+ cells / mm2 Normalized to isotype control
P
Myenteric Plexus
IBA1+ cells / mm2 Isotype control normalized
K
Submucosal Plexus
TH+ cells / mm2 Normalized to isotype control
M
Submucosal Plexus
TH+ area Normalized to CFA only
O
Submucosal Plexus
ANNA1+ cells / mm2 Normalized to isotype control
Q
Submucosal Plexus
IBA1+ cells / mm2 Isotype control normalized

Figure 6

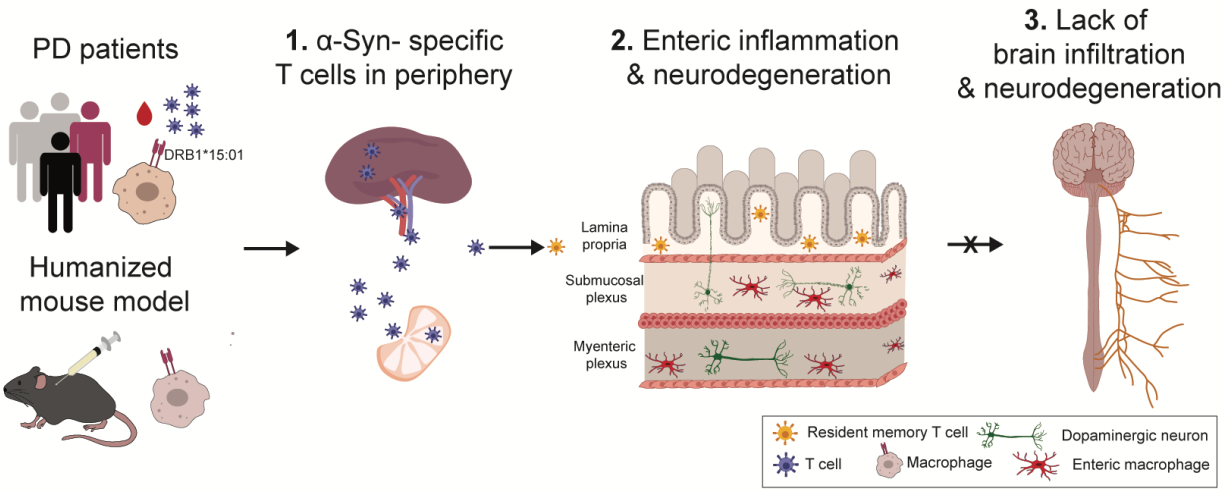
PD patients
DRB1*15:01
Humanized mouse model
1. α-Syn- specific T cells in periphery
2. Enteric inflammation & neurodegeneration
3. Lack of brain infiltration & neurodegeneration
Lamina propria
Submucosal plexus
Myenteric plexus
Resident memory T cell
T cell
Macrophage
Dopaminergic neuron
Enteric macrophage

Figure 7